New lipid nanovesicles
as topical delivery systems for anti - inflammatory drugs

Università degli Studi di Cagliari
PhD Program in Scienze e Tecnologie Farmaceutiche
SDD Chim/09
A.A.: 2012 – 2013 ciclo XXVI

PhD candidate: Ines Castangia
PhD program coordinator: Prof. Elias Maccioni
Supervisor: Prof.ssa Anna Maria Fadda

REGIONE AUTONOMA DELLA SARDEGNA
UNIONE EUROPEA
Fondo sociale europeo
FSE 2007-2013
POR SARDEGNA
obiettivo competitività regionale e occupazione

Ines Castangia gratefully acknowledges Sardinia Regional Government for the financial support of her PhD scholarship (P.O.R. Sardegna F.S.E. Operational Programme of the Autonomous Region of Sardinia, European Social Fund 2007-2013 -Axis IV Human Resources, Objective l.3, Line of Activity l.3.1.)".

TABLE OF CONTENTS

1. INTRODUCTION

1.1. The skin: structure and function

The skin is the largest organ of the human body. The most important function is to form a barrier between the organism and the external environment. In this way the skin protects the individual from environmental influences such as mechanical impacts, ultraviolet light, chemicals, or pathogenic microorganisms and as well as the unregulated loss of water and solutes (*Jadoul, Bouwstra, and Préat 1999) (Thomas and Finnin 2004*) (Figure 1).

Skin consists of three main strata: the hypodermis, is the innermost layer, composed of lipocytes that are arranged into fat lobules separated from one another by fibrous septae, it offers the body thermal and mechanical protection; the upperlying dermis formed by collagen fibres, elastic tissue, ground substance and spread cells, mostly fibroblasts, it contains nerve endings, bood vessels and lymphatic vessels, it high irrigation ensures the nutrition of the skin cells; over the dermis and separated by the basement membrane, the epidermis is composed of different layers, depending on the state of keratinocyte differentiation, where the stratum corneum is the uppermost layer. Keratinocytes are affected by a process of keratinisation, in which the cell differentiates from the basal layer (stratum basale), through the stratum spinosum and stratum granulosum, to the stratum corneum (*Sinico and Fadda 2009*). (Figure 1)

Thus, the stratum corneum represents the physical epidermal barrier against the percutaneous penetration of chemicals and microbes and is capable of withstanding mechanical forces. The final steps in keratinocytes differentiation are associated with profound changes in their structure, resulting in this into anucleated and flattened cells, called corneocytes. These are densely packed within the extracellular lipid matrix which is arranged in bilayers, often called "brick and mortar" arrangement, where the protein rich corneocytes represent the bricks and the lipid matrix, the mortar, originally described by Michaels et al. 1975 (*Michaels,*

Chandrasekaran, and Shaw 1975). (Figure 3)

At the ultrastructural level, both the bricks and the mortar components of the paper-thin stratum corneum have incredible structural and functional complexity, metabolic adaptations and ability for autopoesis (self-maintenance by constant renewal).

The protein envelop contributes to the biomechanical properties of the stratum corneum as a result of cross-linking of specialized cornified envelope structural proteins, including loricrin, involucrin and trichohyalin. The mortar lipids filling the tortuous pathway between the stacked corneocytes: a highly complex mixture of about 13 species of ceramides, cholesterol, and free fatty acids, these provide the permeability barrier. Ceramides are approximately 50% of the total lipid mass and responsible of the lipid organization. Cholesterol (25%) improves the mixing of the different lipid compounds. The free fatty acids (10%) are mainly saturated with a chain length of 20 carbon atoms or

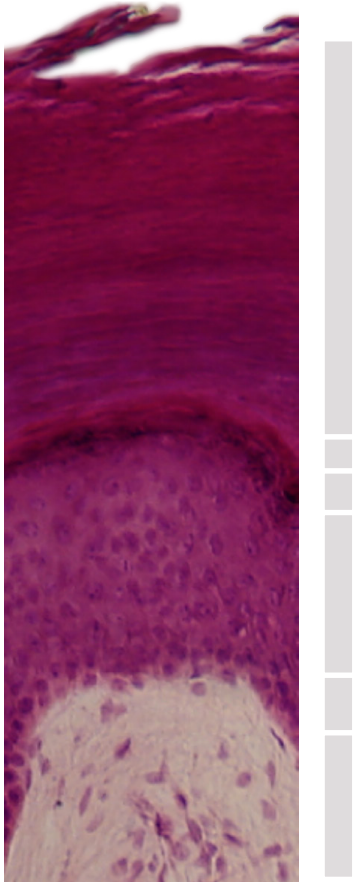

Figure 1. Layer of the skin

Figure 2. Schematic diagram of the epidermis.

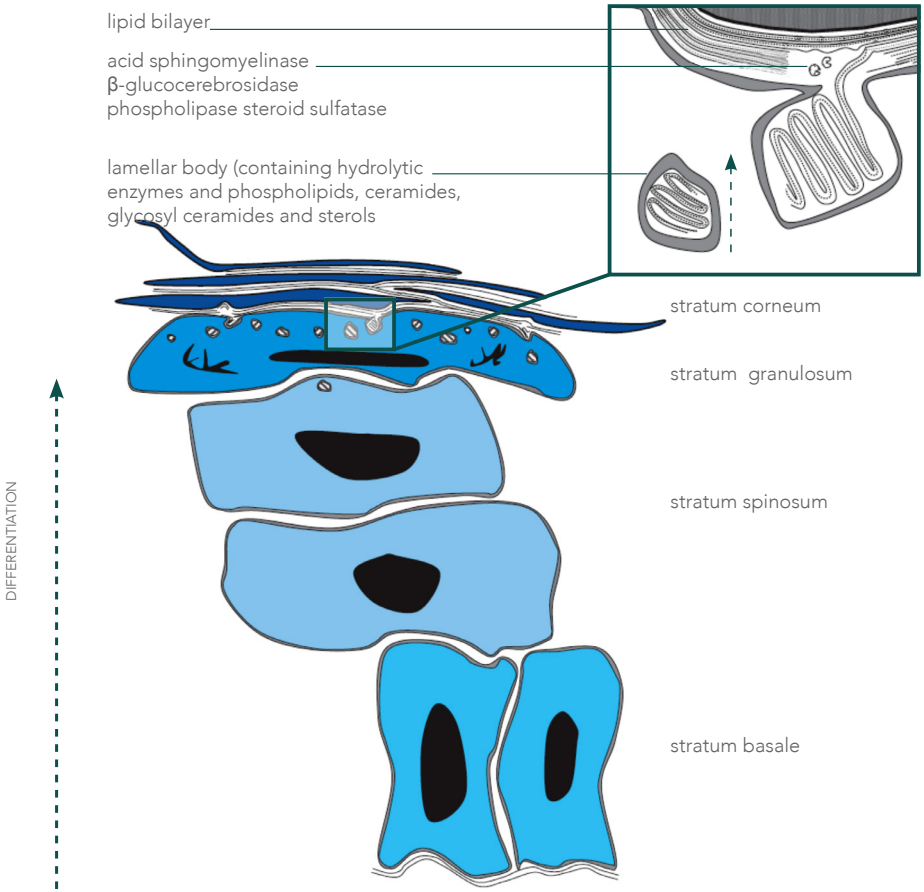

more, with additional smaller fractions of oleic and linoleic acids.
The nucleated epidermis also contributes to the barrier through tight, gap and adherens junctions, as well as through desmosomes and cytoskeletal elements. During epidermal differentiation lipids are synthesized in the keratinocytes and extruded into the extracellular domains, where they form extracellular lipid-enriched layers. The cornified cell envelope, a tough protein/lipid polymer structure, resides below the cytoplasmic membrane on the exterior of the corneocytes. Ceramides A and B are covalently bound to cornified envelope proteins and form the backbone for the subsequent addition of free ceramides, free fatty acids and cholesterol in the stratum corneum. Filaggrin is cross-linked to the cornified envelope and aggregates keratin filaments into macrofibrils.
Formation and maintenance of barrier function is influenced by cytokines, cyclic adenosine monophosphate and calcium. Changes in epidermal differentiation and lipid composition lead to a disturbed skin barrier, which allows the entry of environmental allergens, immunological reaction and inflammation in atopic dermatitis. A disturbed skin barrier is important for the pathogenesis of contact dermatitis, ichthyosis, psoriasis and atopic dermatitis.

Figure 3: Barrier function of the epidermis

1.2. Vesicular carriers

The skin represents an ideal site for drug administration in terms of non-invasive application, offering some advantages over classical oral dosage forms, such as reduction of drug systemic toxicity, improvement of local activity and patient compliance.
Recently, it has become evident that the use of nanocarriers to deliver drugs to the skin increases penetration and permeation through the stratum corneum, but they can also be exploited to localize the drug upon topical treatment. Rationally-designed nanocarriers may improve the therapeutic index of drugs, by modifying their pharmacokinetic and biodistribution (*Jadoul et al. 1999; Thomas and*

brick=corneocyte
mortar=Lipid (Membrane bilayers)

Finnin 2004)(*Sinico and Fadda 2009*).

Among the several nanosystems in the pharmaceutical panorama, phospholipid vesicles, namely liposomes, have been extensively studied (figure 4). Many studies show that skin deposition of phospholid vesicles is affected by a number of factors, such as lipid composition, vesicle structure and the thermodynamic state of the lipid bilayer. Several authors have been showing that the modification of lipid vesicle composition can lead to elastic, deformable and/or soft vesicles that have superior ability to enhance dermal and transdermal drug delivery with respect to conventional liposomes. Therefore, a great deal of innovative lipid vesicles has been introduced, such as transfersomes and ethosomes, which are reported to have superior skin penetration ability. thus enhancing drug bioavailability and prolonging their efficacy, via non-invasive routes (*Muzzalupo et al. 2011; Sinico and Fadda 2009; Touitou et al. 2000*).

1.2.1. Penetration enhancer containing vesicles (PEVs)

More recently, the group of Technologies of the University of Cagliari has been studying the delivery of drugs by new phospholipid vesicles, named Penetration Enhancer-containing Vesicles (PEVs), which are liposomes containing in their composition a penetration enhancer molecule, capable of influencing vesicle performances and transdermal drug delivery. (figure 5). Vesicles have been prepared following different methods, using several phospholipids and drugs, and various penetration enhancers differing in physicochemical properties and mechanism of skin penetration enhancement. Effective and appropriate PEV formulations have been obtained with the aim of reaching an efficient delivery of different drugs (e.g. tretinoic acid, minoxidil, diclofenac and quercetin) to skin or subcutaneous tissue (*Caddeo et al. 2012; Chessa et al. 2011; Manconi et al. 2009; Manconi, Caddeo, et al. 2011; Manconi, Sinico, et al.*

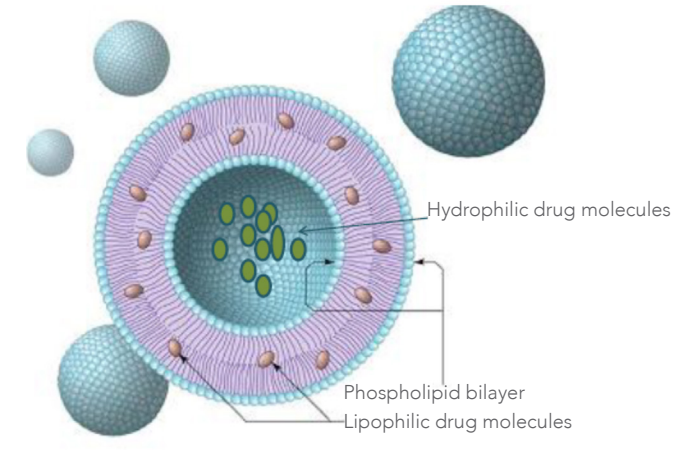

Figure 4: Structure of phospholipid vesicles: liposomes.

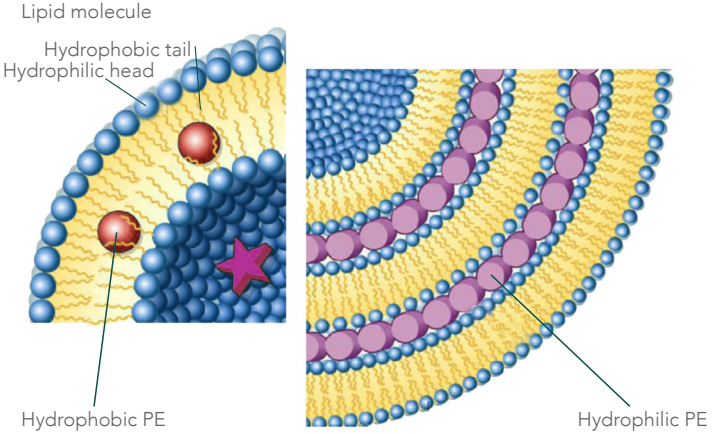

Figure 5: Structure of PEVs

2011; Mura et al. 2009, 2011).

In this framework, considerable attention has been devoted to studying the ability of the PEVs to entrap anti-inflammatory drugs and to enhance their in vitro and in vivo efficacy in the local treatment of various inflammatory diseases.

1.3. Inflammation

Inflammation is an essential protective process for preserving the integrity of organisms against physical, chemical infective and autoimmune causes. However, it is frequent that the inflammatory response to several insults erroneously leads to the damaging of normal tissues due to an overproduction of reactive oxygen species (ROS), nitric oxide (NO) and cytokines, such as tumor necrosis factor-alpha (TNF-α) (Manconi, Caddeo, et al. 2011).

Therapeutic treatments involve the care of symptoms by stopping the anti-inflammatory process and, if possible the native cause. Usually, inflammation is localized in a specific organ or apparatus, like skin, subcutaneous tissue, muscular or osteoarticular apparatus, and it can often become chronic (figure 6). Long-term systemic cures with steroidal or non-steroidal anti-inflammatory drugs can cause the onset of several side effects and a low drug bioavailability at the site of action (*Tavano, Muzzalupo, Trombino, et al. 2010*).

Cutaneous administration represents a valid alternative to systemic treatment of local inflamed skin or muscle. In particular, the nanoencapsulation of anti-inflammatory drugs can improve their local bioavailability and efficacy minimizing side effects. Among different nanocarriers, phospholipid lamellar vesicles are one of the most versatile systems for the improvement of skin penetration and permeation of drugs. Different anti-inflammatory drugs have been successfully included within phospholipid vesicles (e.g., liposomes, transfersomes, and ethosomes) to efficiently enhance their transdermal delivery (*Sinico and Fadda 2009*).

Diclofenac (DCF) is one of the most po-

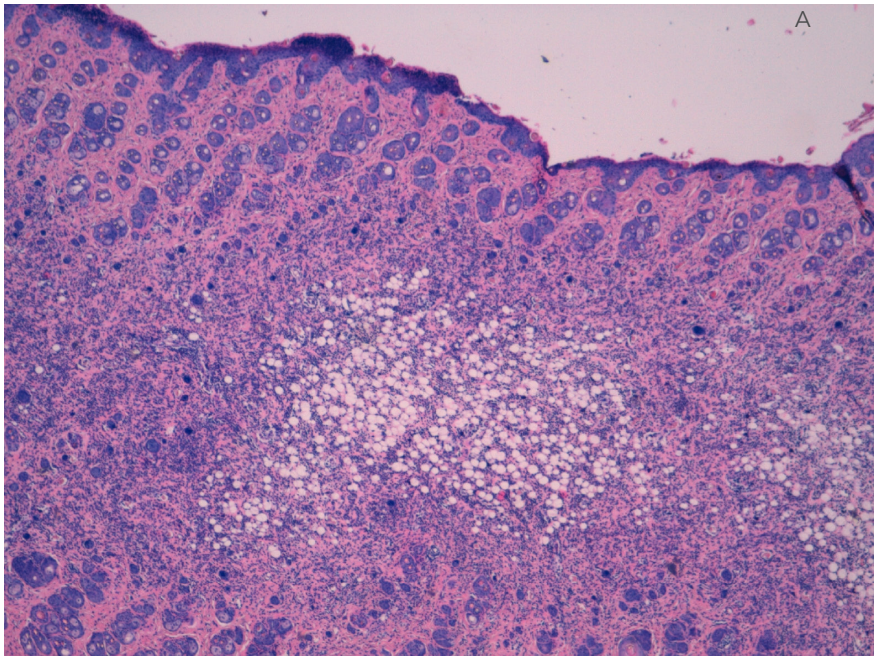

Figure 6: Representative histological sections of skin: A) inflamed skin and B) healthy skin.

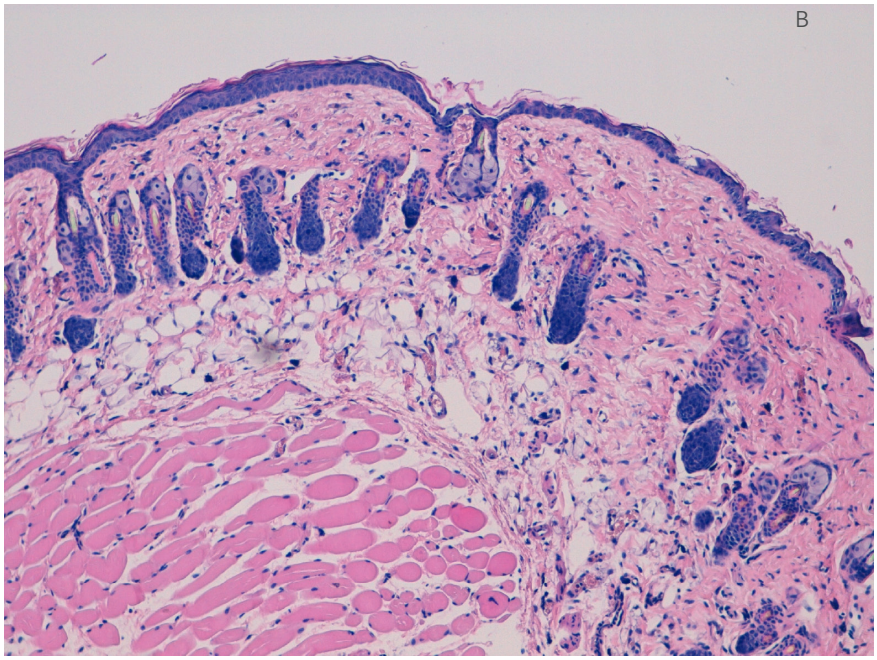
B

tent and commercially successful non-steroidal anti-inflammatory drugs (NSAIDs), very often used in transdermal drug delivery. Due to several drawbacks when orally given, topical administration is preferable for diclofenac in long-term cures, such as treatment of local muscle inflammation, although the drug shows low skin permeability. Different penetration enhancers have been employed to increase its percutaneous absorption, as they reversibly reduce the skin barrier resistance (Mura et al. n.d.)(*Mura et al. 2011*).

Alternatively to conventional NSAIDs, natural and safe anti-inflammatory drugs, such as polyphenols, flavonoids and cumarins, are being proposed to be encapsulated in phospholipid vesicles and administered to the skin. Flavonoids are a group of naturally occurring polyphenolic compounds that are found in most plants and are reported to have a significant impact on the inflammatory process. Curcumin (CUR) and quercetin (QUE) are among the most widely distributed flavonoids, and have demonstrated to possess potent anti-oxidant, anti-inflammatory and anti-carcinogenic activities. They control the formation of proinflammatory mediators, such as prostaglandins and leukotrienes. Curcumin has been shown to reduce edema in rats and to moderately reduce the clinical symptoms in rheumatoid arthritis patients. Quercetin inhibits mast cell degranulation, release of histamine and also inhibits phospholipase A2, cyclooxygenase and lipoxygenase activity. Although previous studies suggest that both curcumin and quercetin have significant anti-inflammatory and anti-allergic properties, unfortunately the efficacy of these natural antioxidants is limited by low in vivo bioavailability, which limits their potential health benefits (*Scalia and Mezzena 2009*)(*Montenegro et al. 2007*)(*Vicentini et al. 2008*)(*Hjorth Tønnesen et al. 1993; Subramanian et al. 1994*)

2. AIM OF THE WORK

Topical drug delivery has gained increased importance for anti-inflammatory drug delivery and several methods have been proposed to improve drug localization into the skin and inflamed tissues in order to enhance drug bioavailability as well as to reduce systemic side effects. Among the several proposed methods, the use of nanoparticulate carries has shown a great deal of interest with different and new nanovesicular carriers introduced by different research teams. Moreover, the liposomal carriers have the capability to vehiculate drugs with low water solubility, to protect them from environment and also to improve cutaneous delivery of drugs with low skin permeability.

Therefore, the purpose of the present study was to formulate new vesicular carriers to optimize the topical delivery of anti-inflammatory drugs:

- diclofenac sodium salt,
- quercetin,
- curcumin.

These drugs are characterized by different molecular structures and, this, different physico-chemical properties.

In particular, diclofenac shows several drawbacks when orally given but its topical delivery is limited by low skin permeability. Topical bioavailability of quercetin is hindered by its poor solubility in aqueous media and low skin permeability while the poor hydro-soluble curcumin is also photosensible and instable.

Therefore, their incorporation into innovative vesicles, PEVs, also containing a penetration enhancer could be a useful tool to improve their performance. Therefore, in this study new PEVs, different for composition and/or lipid concentration, have been prepared using glycol penetration enhancers to evaluate their aptitude as topical carriers to efficiently deliver these drugs to the skin allowing the drug to reach therapeutic levels into inflamed fibroblasts. The formulations were fully characterized from the physico-chemical and technological point of view while their properties as carriers were evaluated by in vitro and in vivo experiments.

Figure 1: Chemical structure of (A) Diclofenac, (B) Quercetin and (C) Curcumin.

A

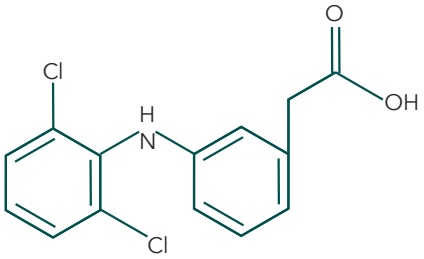

B

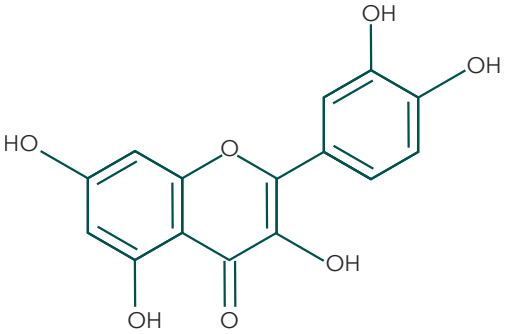

C

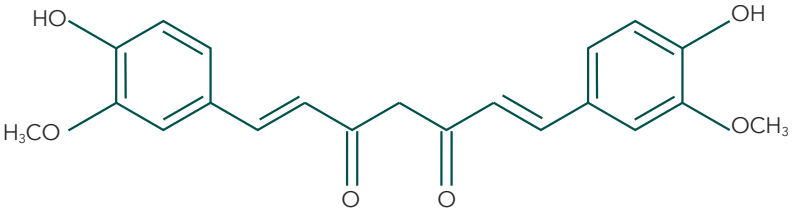

3. CLOSE - PACKED VESICLES FOR DICLOFENAC SKIN DELIVERY AND FIBROBLAST TARGETING

Published in Colloids and Surfaces B: Biointerfaces 111, 609-617, 2013

3.1. Introduction.

Topical delivery of drugs has several advantages over other traditional routes of administration, including improved bioavailability for drugs that suffer gastrointestinal environment and/or hepatic first effects. However, the barrier nature of the stratum corneum (SC) represents a significant obstacle for most drugs to be delivered into and through the skin using the classical dosage forms such as creams, ointments, and gels. To overcome the barrier properties of the SC and enhance drug transport across intact skin, several techniques have been developed (*Jadoul et al. 1999; Sinico and Fadda 2009; Thomas and Finnin 2004*). One of the approaches especially studied in the last decades is the use of lipid nanocarriers, such as innovative liposomal vesicles (*Cosco et al. 2008; Muzzalupo et al. 2011; Tavano, Muzzalupo, Cassano, et al. 2010*). Introduction of these delivery systems in nanomedicine has several advantages that include safety of the carrier, its capability to enhance drug delivery into/through the skin as well as to deliver the drug to its therapeutic target while reducing drug toxicity. Diclofenac (DCF), a phenyl acetic acid derivative, is a potent member of the non-steroidal anti-inflammatory drugs (NSAIDs), frequently used for treatment of rheumatic disorders and other chronic inflammatory diseases. In chronic inflammations, such as arthritis, fibroblasts are the source of anti-inflammatory mediators and contribute to disease persistence in a defined anatomical location. Fibroblasts show a disordered behavior that causes an excessive survival and accumulation of leukocytes within inflamed tissues *(Manconi, Caddeo, et al. 2011)*. They are responsible for tissue injury and cartilage invasion in the presence of inflammatory infiltrates. Therefore, topical DCF delivery could be useful to reduce the drug systemic toxicity while improving its local efficacy *(Tavano, Muzzalupo, Trombino, et al. 2010)*. The use of vesicular drug delivery systems, such as liposomes, niosomes, ethosomes, and transfersomes, may en-

hance DCF delivery into and through the skin allowing the drug to reach therapeutic levels into inflamed fibroblasts *(Battaglia and Ryan 2005; Caddeo et al. 2008; Manconi et al. 2003, 2005; Manconi, Sinico, et al. 2011)*. In previous works, we prepared and tested penetration enhancer-containing vesicles (PEVs) as promising carriers for enhanced (trans)dermal delivery of diclofenac, in the form of either acid or sodium salt *(C. Mura et al. 2011; Mura et al. 2009)*. In the present work, we propose concentrated and close-packed PEVs prepared using a high concentration (180 mg/ml) of a commercial lipid mixture containing phosphatidylcholine, phosphatidylethanolamine, fatty acids and triglycerides (Phospholipon®, P50) and Transcutol® P (Trc) mixed at different ratios (10, 20, 30%, v/v) with phosphate buffer solution (PBS, pH 7). Trc is a water miscible, atoxic, and biocompatible penetration enhancer (PE). Diclofenac (DCF) was incorporated in transcutol-PEVs and conventional liposomes, which were used as control. Vesicles were characterized in term of morphology, size distribution, zeta potential, stability, lamellarity, and ability to promote ex vivo diclofenac skin delivery. The cytotoxic activity of empty and DCF-loaded vesicles was evaluated toward mouse 3T3 fibroblasts grown as confluent monolayer. Vesicle cell interactions and cellular uptake were evaluated by fluorescence microscopy using vesicles labeled with the lipophilic marker 1,2-dioleolyl-sn-glycero-3-phosphoethanolamine-N-(lissamine rhodamine B sulfonyl) (Rho-PE) and loaded with the hydrophilic probe 5(6)-carboxyfluorescein (CF).

3.2. Materials and methods

3.2.1. Materials

Phospholipon® 50 (P50) containing phosphatidylcholine (45%), phosphatidylethanolamine (10–18%), fatty acids (7%) and triglycerides (3%) was a gift from AVG S.r.l. (Milan, Italy); 1,2-dioleolyl-sn-glycero-3-phosphoethanolamine-N-(lissamine rhodamine B sulfonyl) (Rho-PE) was pur-

chased by Lipoid GmbH (Ludwigshafen, Germany). 2-(2-Ethoxyethoxy)ethanol (Transcutol® P, Trc) was donated from Gattefossé (Saint Priest, France). Phosphate buffer solution (PBS, pH 7) was purchased from Carlo Erba Reagents (Rodano, Italy). DCF sodium, 5(6)-carboxyfluorescein (CF) and all the other products were purchased from Sigma–Aldrich (Milan, Italy). DCF free acid (DCF) was obtained by acidic precipitation from a solution of diclofenac sodium *(Manconi et al. 2009; Manconi, Caddeo, et al. 2011)*.

3.2.2. Vesicle preparation

Liposomes and PEVs, were prepared weighing P50 (180 mg/ml), DCF (10 mg/ml) and hydrating them with PBS or Trc/PBS solution (10, 20 and 30%, v/v) to obtain liposomes or PEVs. Dispersion was sonicated for 2 min with a Soniprep 150 ultrasonic disintegrator (MSE Crowley, London, United Kingdom) *(Caddeo et al. 2008; Manconi et al. 2003, 2005)*.

Vesicle dispersions were purified from the non-incorporated drug by dialysis loading them into dialysis tubing (Spectra/Por® membranes, 3 nm pore size; Spectrum Laboratories Inc., Rancho Dominguez, CA, United States) and dialyzing against PBS at 5°C for 2 h. Drug loading efficiency (E%), expressed as the percentage of the amount of drug initially used, was determined by high performance liquid chromatography (HPLC) after disruption of vesicles with Triton X-100. DCF content was quantified at 227 nm using a chromatograph Alliance 2690 (Waters, Milano, Italy). The column was a Symmetry C18 (3.5 µm, 4.6 mm × 100 mm, Waters, Milano, Italy). The mobile phase was a mixture of 30% water and 70% acetonitrile (v/v), delivered at a flow rate of 0.5 ml/min *(Caddeo et al. 2008; Manconi et al. 2003, 2005)*.

3.2.3. Vesicles characterization

Vesicles were characterized by Transmission Electron Microscopy (TEM) for vesicle formation and morphology. Samples

were examined with a JEM-1010 (Jeol Europe, Paris, France) transmission electron microscope equipped with a digital camera MegaView III and Software "Analysis", at an accelerating voltage of 80 kV. The average diameter and polydispersity index (P.I.) of the samples were determined by Photon Correlation Spectroscopy (PCS) using a Zetasizer nano (Malvern Instrument, Worcestershire, United Kingdom). Zeta potential was estimated using the Zetasizer nano by means of the M3-PALS (Phase Analysis Light Scattering) technique. All the samples were analyzed 24 h after their preparation. A stability study was performed by monitoring the vesicle average size and zeta potential over 90 days at 4 ± 2 C.

3.2.4. X-ray diffraction

Vesicle structure was studied by small and wide-angle X-ray scattering (SWAXS). SAXS and WAXS patterns were recorded simultaneously using a S3-MICRO SWAXS camera system (HECUS X-ray Systems, Graz, Austria). The working q-range was 0.003–0.6 Å−1, where $q = (4\pi \sin\theta)/\lambda$ is the modulus of the scattering wave vector, θ the scattering angle and λ the wavelength. The diffraction patterns were recorded at 25 C. All scattering curves were reproduced twice with subsequent calculation of the electron distance distribution, and yielded identical results. For the figures, a representative curve was selected, plotting the scattering intensity (I) as a function of the scattering vector (q). SAXS patterns were analyzed using the program GAP (Global Analysis Program) developed by Pabst (Battaglia and Ryan 2005; Pabst et al. 2003). The analysis technique models the full q-range in the SAXS regime, including Bragg peaks and diffuse scattering. The GAP allows fitting the SAXS pattern of bilayer-based structures, i.e. vesicles and lamellar phases. From the analysis, the membrane thickness was obtained through the definition $dB = 2(zH + \sigma H)$. zH derives from SAXS curve fitting with GAP, while σH was kept fixed at 3 Å.

3.2.5. Rheological analysis

Steady shear tests and dynamic oscillatory tests were performed with a controlled strain and stress rheometer (Kinexus pro, Malvern Instrument, Worcestershire, United Kingdom) equipped with an rSpace data acquisition software. Analyses were carried out using a double-gap concentric cylinder. The double-gap configuration is useful for low viscosity dispersions. Viscometry experiments were conducted in a shear range of 0.01–10 Pa. All samples were subjected to an initial amplitude sweep to determine the linear viscoelastic region where the values of the moduli are independent of the applied deformation. Subsequent frequency sweep tests were performed from 0.01 to 10 Hz, and at a shear stress of 0.5 Pa. The oscillatory parameters used to compare the viscoelastic properties of the different dispersions were the storage modulus (G′) and the loss modulus (G″). All measurements were made in triplicate, at a constant temperature of 25 ± 2 C.

3.2.6. Ex vivo skin penetration and permeation studies

Experiments were performed non occlusively by means of Franz diffusion cells (diffusion area of 0.785 cm2), using new born skin of Goland–Pietrain hybrid pigs (1.2 Kg), provided by a local slaughterhouse and used within 24 h after excision. Skin was kept at 4 C and, 12 h before the experiments, it was pre-equilibrated in PBS solution at 37 °C. Skin specimens (n = 6) were sandwiched securely between donor and receptor compartments of the Franz cells, with the stratum corneum (SC) side facing the donor compartment. The receptor compartment was filled with 5.5 ml of PBS solution, which was continuously stirred and thermostated at 37 ± 1 °C to reach the physiological skin temperature (i.e. 32 ± 1 °C). 100 µl of the samples was placed onto the skin surface. At regular intervals (1, 2, 4, 6, 8 h) the receiving solution was withdrawn and analyzed by HPLC for drug content (as described in Section 2.2).

After 8 h, the skin surface of specimens

was washed and the SC was removed by stripping with adhesive tape Tesa AG (Hamburg, Germany). The epidermis was separated from the dermis with a surgical sterile scalpel. Tape strips, epidermis, and dermis were placed each in methanol, sonicated to extract the drug, and then assayed for drug content by HPLC (see Section 2.2).

3.2.7. Cell cultures

Mouse 3T3 fibroblasts (ATCC collection) were grown as confluent monolayer at 37 °C in phenol red-free Dulbecco's Modified Eagle's medium (DMEM) (Life Tecnologies Europe, Monza, Italy) with high glucose, supplemented with 10% (v/v) fetal bovine serum, penicillin (100 U/ml), and streptomycin (100 µg/ml) (Life Technologies Europe, Monza, Italy) in 5% CO2 incubator at 37 °C.

3.2.8. Cell viability studies (MTT assay)

3T3 cells were plated into 24-well plates at a density of 5 × 104 cells/well. After 24 h of incubation, 3T3 cells were treated for 2, 4, 8, 24 and 48 h with empty vesicles or DCF-loaded vesicles or DCF solution (50 µl of formulation in 500 µl of medium). Cell viability was determined by the MTT [3(4,5-dimethylthiazolyl-2)-2,5-diphenyltetrazolium bromide] colorimetric assay. Briefly, 500 µl of MTT reagent (0.5 mg/ml in PBS) was added to each well and after 2 h the formed formazan crystals were dissolved in DMSO. The reaction was spectrophotometrically measured at 570 nm with a microplate reader (Synergy 4, ReaderBioTek Instruments, AHSI S.P.A, Bernareggio, Italy). All experiments were repeated at least three times and in triplicates. Results are shown as percent of cell viability in comparison with non-treated control cells (100% viability).

3.2.9. Cellular uptake of RhoPE labeled CF loaded vesicles

The cell interactions and cellular uptake were investigated by fluorescence microscopy using vesicles labeled with a lipophilic fluorescent marker 1,2-dioleolyl-sn-glycero-3-phosphoethanola-

mine-N-(lissamine rhodamine B sulfonyl) (0.035 mg/ml; Rho-PE) and loaded with a hydrophilic fluorescent marker 5(6)-carboxyfluorescein (0.025 mg/ml; CF). Vesicles were purified from the non-entrapped markers by dialysis (see Section 2.2). 3T3 cells were grown in 35 mm dishes and experiments were carried out two days after seeding when the cells became confluent and stopped dividing due to contact inhibition. Cells were incubated at 37 °C with RhoPE labeled CF loaded vesicles (50 µl of formulation in 500 µl of medium) for 2, 4 and 8 h. Before observations, cells were washed twice with DMEM to remove fluorescent vesicles and background fluorescence, and then loaded with 650 µl nuclear stain Hoechst 33258. The adopted filters allowed for a virtually complete separation of the emissions and the simultaneous observation of CF (green dye), Rho-PE (red) and Hoechst (blue) in live cells. In control experiments, cells incubated with free CF at the same concentration of that used in the preparation of vesicle dispersions did not display any appreciable fluorescence, confirming that the free CF does not permeate cell plasma membranes.

3.2.10. Fluorescence microscopy and image analysis

Light microscopy observations were made using a Zeiss (Axioskop, Zeiss, Oberkochen, Germany) equipped with 20× and 40×/0.75 and a HBO 50W L-2 mercury lamp (Osram, Berlin, Germany). Twelve images were acquired with a CCD camera (QICAM, Q imaging, Canada). CF, Rho-PE and Hoechst 33258 fluorescence was observed with 470 ±20/ 535 ±40, 546±6/ 620 ±60 and 360 ±20/ 460 ± 25 excitation/emission filters respectively. For quantification of intracellular fluorescence intensity, acquired images were processed for background subtraction and a 3 × 3 median filter was applied in order to flatten noise variations. The value related to the pixel pointed by the mouse was recorded as fluorescence intensity (arbitrary units). Digital images were analyzed and image alignments

were obtained with Image Pro Plus software (Media Cybernetics, Silver Springs, MD). Calculations were made with Excel (Microsoft Co., Redmond, WA).

3.2.11. Statistical analysis of data

Data analysis was carried out with the software package R, version 2.10.1. Results are expressed as the mean ± standard deviation. Multiple comparisons of means (Tukey test) were used to substantiate statistical differences between groups, while Student's t-test was used for comparison between two samples. Significance was tested at the 0.05 level of probability (p).

3.3. Results and discussion

3.3.1. Vesicles characterization

In previous studies, different penetration enhancers (PEs, transcutol, propylen glycol, labrasol and oramix) were used to prepare alternative phospholipid vesicles (PEVs) as carriers for (trans)dermal delivery of different model drugs (*Manconi et al. 2003, 2009; Manconi, Caddeo, et al. 2011; Manconi, Sinico, et al. 2011; C. Mura et al. 2011; Mura et al. 2009*). Results underlined PE capability of influencing vesicle physicochemical properties and enhancing (trans)dermal drug delivery. In the present work, new concentrated and interconnected P50-PEVs, containing increasing amounts of Trc (10%, 20%, 30%), were tested ex vivo in comparison with P50-liposomes (control). P50 (180 mg/ml) was used to prepare stable vesicles loading 10 mg/ml of DCF. This concentration was needed to avoid drug precipitation and vesicle instability. Moreover, all these highly lipid concentrated vesicles strongly interacted each other forming interconnected and densely packed vesicles mixed to other bilayered structures (Battaglia and Ryan 2005). However, when diluted in water or applied onto the skin, they are able to maintain their structure and size but, within minutes, convert to single vesicles as confirmed by TEM micrographs. As an example, Figure 1a shows a TEM picture of 10% Trc-PEVs,

Figure 1. Negative stain electron micrographs of DCF-loaded vesicles before (a) and after few minutes of water dilution (b) 10% Trc-PEVs, (c) 20% Trc-PEVs (d) 30% Trc-PEVs.

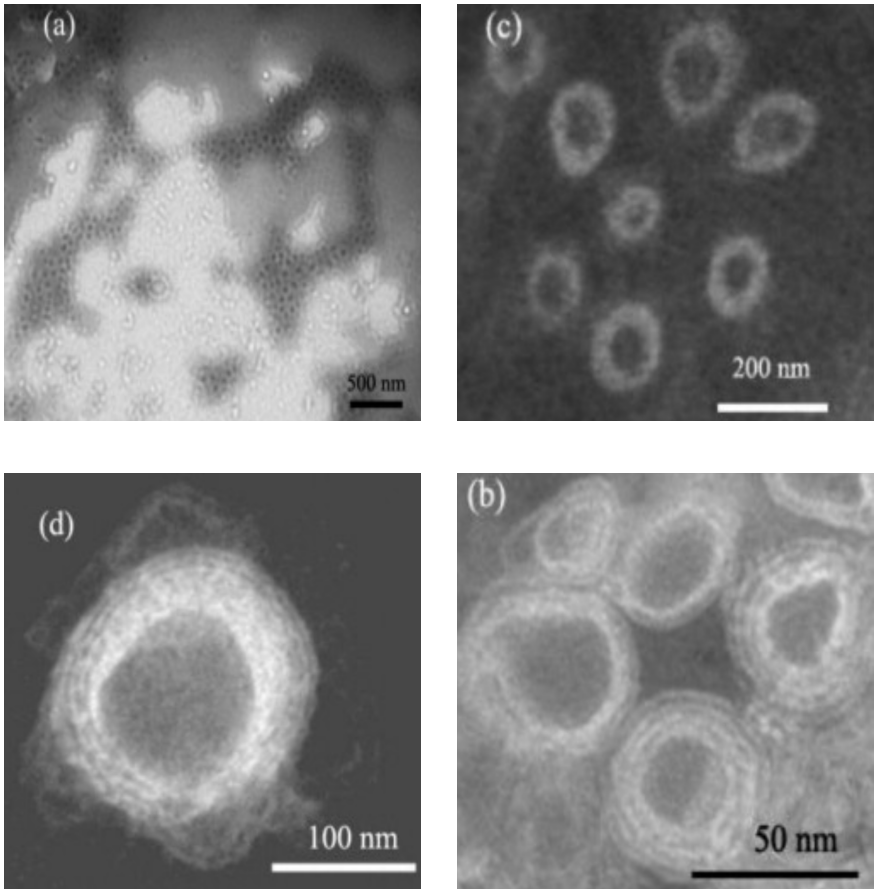
(a)
500 nm
(c)
200 nm
(d)
100 nm
(b)
50 nm

Sample		Size (nm)	PI	ZP (mV)	E (%) DCF
Liposomes	empty	84 ± 7	0.22	-49 ± 2	
10% Trc-pevs		109 ± 6	0.21	-67 ± 3	
20% Trc-pevs		253 ± 11	0.27	-70 ± 3	
30% Trc-pevs		136 ± 5	0.16	-75 ± 4	
Liposomes	DCF	75 ± 9	0.23	-61 ± 3	-77 ± 4
10% Trc-pevs		97 ± 3	0.20	-72 ± 5	-70 ± 5
20% Trc-pevs		220 ± 15	0.25	-76 ± 2	-57 ± 4
30% Trc-pevs		162 ± 9	0.18	-81 ± 4	-48 ± 6

Table 1. Average size, polydispersity index (PI), zeta potential (ZP) of empty and DCF-loaded liposomes and PEVs, incorporation efficiency (E%) of DFC. Each value is the mean ±SD of at least four experimental determinations

where close and interconnected multilamellar vesicles are clearly evident together with lamellar ribbons. Upon dilution, all systems evolve to single multilamellar (Figure 1b and d, 10 and 30% Trc-PEVs, respectively) or unilamellar vesicles as shown in Figure 1c for 20% Trc-PEVs.

Results of vesicle characterization, in terms of mean size, polydispersity index (PI), and zeta potential values are shown in Table 1. For all formulations, vesicle mean size ranged from 75 to 253 nm with a fairly narrow size distribution (PI 0.16–0.27). Results indicated that the particle diameter was strongly affected by the presence of Trc but not by the drug. In fact, drug entrapment did not statistically change the average size of all vesicles, except for 20% Trc-PEVs, whose mean diameter statistically decreased in the presence of DCF. The Trc effect was more evident: PEVs were always larger than control liposomes, in particular 20% Trc-PEVs showed the highest average size. This is probably due to an increased hydration of the lipid membrane surface in the presence of Trc with a consequent modification of bilayer swelling or Trc could have interpenetrated the lipid hydrocarbon chains causing a modification in packing assembly (*McDaniel, McIntosh, and Simon 1983*). Vesicle surface charge primarily depends on the lipid composition: the main P50 component is phosphatidylcholine, a zwitterionic compound that at pH 7.0 carries a negative charge, as well as the fatty acids (7% in the P50-mixture). Therefore, a negative charge in all formulations was observed. The negative charge increased with the addition of Trc and DCF from −49 mV for empty liposomes to −81 mV for DCF-loaded 30% Trc-PEVs. PEVs always showed a negative zeta potential value higher than that of control liposomes and empty vesicles. Control liposomes were able to incorporate DCF in good yields (77%), always higher than those of PEVs that showed a drug loading capacity (E%) that decreased when Trc increased, varying between 48% and 70% (Table 1).

Figure. 2. (a) Small angle X-ray diffraction (SAXS) patterns and maximum q value of scattering curve of DCF-loaded liposomes and PEVs. (b) Storage (G′) and loss (G″) moduli against frequency of liposomes and PEVs.

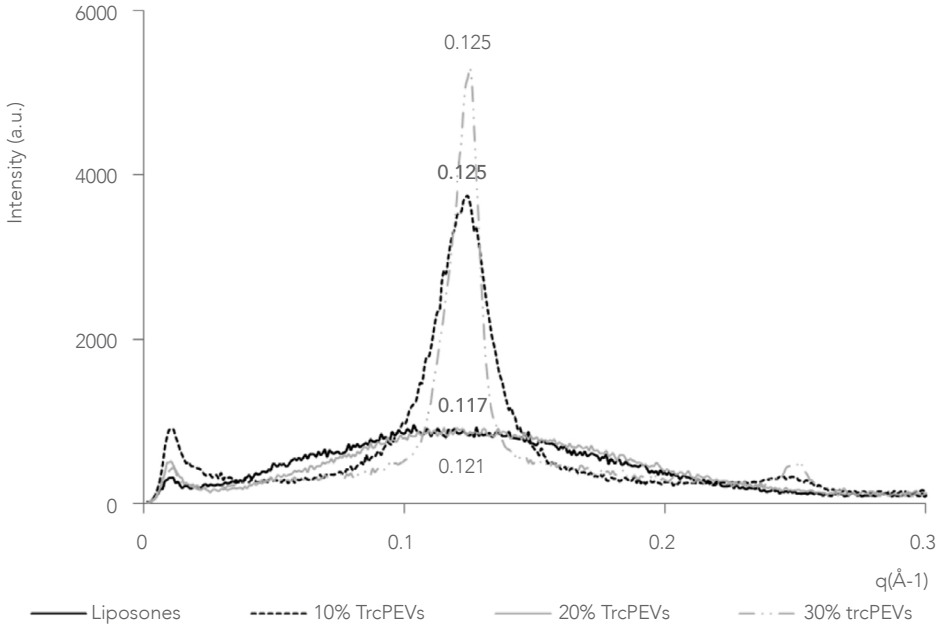

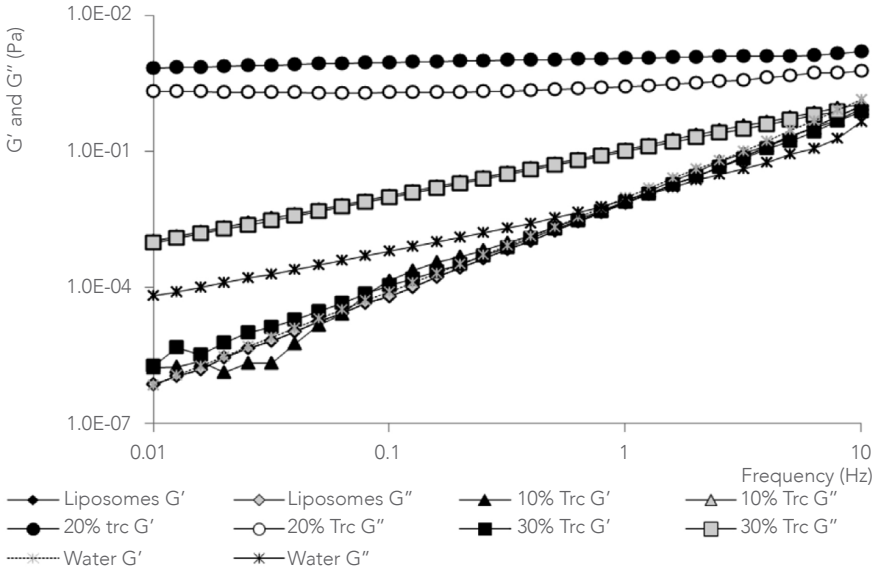

3.3.2. Small-angle X-ray scattering

Vesicle structure was confirmed by small-angle X-ray scattering (SAXS). SAXS scattering curves of intensity (I) versus wave vector (q) for control liposomes and PEVs are shown in Figure 2 (a). Liposome curve presented a diffuse scattering, with a weak (q~0.117 Å−1), no sharp but distinctive single peak indicating the presence of unilamellar vesicle with bilayer thickness of (dB) 47.4 Å. 10% Trc-PEVs displayed a sharp diffraction first order peak, at higher q value (0.125 Å−1) and a lower second order peak indicative of multilamellar structures. Increasing Trc percentage to 20%, the peak shifted to lower q values (0.121 Å−1) but became wider and its intensity decreased because the amount of lamellar structures decreased. The signal of 30% Trc-PEVs (fully hydrated lipid membrane) showed a narrow peak and a lower second order peak characteristic of a multilamellar structure (q 0.125 Å−1), distinctly sharper than those from the 10% Trc-PEV dispersion, thus, indicating a larger size of

the lamellar domains in this dispersion (Battaglia and Ryan 2005). Therefore, the tree different Trc concentrations led to a different P50 organization. 10% and 30% Trc produced multilamellar vesicles: 10% Trc addition allowed a structure change in comparison with control liposomes (from uni- to multi-lamellar) but not in bilayer thickness (dB 47.0 Å). Moreover, only a slight increase in vesicle diameter was obtained because Trc improved hydration of the lipid membrane surface with a consequent modification of the inter-lamellar long-range forces and lamellarity; 20% Trc interpenetrated the lipid hydrocarbon chains causing a modification in packing assembly and bilayer thickness (dB 46.4 Å) and, thus, establishing a change of bilayer curvature with a strong improvement of size; 30% Trc addition slightly affected bilayer thickness (dB 47.0 Å) and also the hydration of the lipid membrane surface leading to a simultaneous increase of lamellarity and size (in comparison with control liposomes).

3.3.3. Rheological analysis

Rheological properties of samples depend on strength of particle–particle interactions occurring at supramolecular level and on vesicle deformability at intramolecular level. These, in turns, are affected by the microstructure of the lamellar vesicles. The effect of Trc concentration on the apparent viscosity of vesicle dispersions was first examined. In the plot of shear rate versus shear stress (data not shown), behavior of control liposomes and PEVs (Trc 10% and 30%) is like Newtonian fluids: the shear rate linearly increased when the shear stress increased and the constant of proportionality was the apparent viscosity (=shear stress/shear rate). Vesicle viscosity was higher than that of water (1 mPa s): approximately 5, 19, and 13 mPa s for control liposomes, 10% and 30% Trc-PEVs, respectively, and even higher than that of Trc/PBS solution (30%), which was about 3 mPa s. Viscosity increase is due to the existence of interconnected and densely packed lamellar vesicles that fill up a dif-

ferent hydrodynamic volume fraction. Using Trc 20%, the viscosity of PEVs drastically increased, reaching higher orders of magnitude (53 mPa s) and showing a plastic behavior with yield-stress values (data not shown). Additionally, the storage (G') and the loss (G") moduli of all samples were determined by oscillating rheological measurements (Fig. 2b). The oscillatory experiments emphasize a change of the viscoelastic behavior in the presence of 20% Trc in the vesicle dispersion. Control liposomes and 10% and 30% Trc-PEVs showed the same rheological behavior of water, a purely viscous fluid: loss modulus was higher than storage modulus but they were more viscous than water due to their densely packed vesicles. On the contrary, 20% Trc-PEVs showed an inversion of behavior where the storage modulus predominated over the loss modulus and both moduli were higher than those of other vesicles. Therefore, the system behaves like a soft gel. Presumably, this indicates that control liposomes, 10% and 30% Trc-PEVs were densely packed small (75–150 nm) uni- or multi-lamellar vesicles occupying a low volume fraction while Trc 20% PEVs were densely packed and strongly interconnected larger unilamellar (253 nm) vesicles with an increased volume fraction (*Chessa et al. 2011*). This change in the microstructure induced a modification at the supramolecular level: large and multilamellar vesicles (high volume fraction) and high lipid concentration (densely packed vesicles) produced a reduction of free water between vesicles and an increased strength of particle–particle interactions, and, as a consequence, the system became elastic with a yield value.

3.3.4. Ex vivo permeation studies

The skin penetration ability of vesicle-loaded DCF was evaluated by ex vivo experiments through new born pig skin. The amount of drug accumulated into stratum corneum, epidermis and dermis is expressed as the percentage of the drug applied onto the skin (Figure 3 (a)). Ex vivo (trans)dermal experiments

showed an improved skin deposition of DCF when PEVs were used, mostly 10% and 20% Trc-PEVs that enhanced drug deposition two times more than conventional liposomes reaching 16–17% of drug accumulated into the whole skin. Using 30% Trc-PEVs, DCF skin deposition was lower (12%) than that of other Trc-PEVs, as previously found for DCF loaded P90-PEVs (6). Cumulative amounts of permeated drug (μg/cm2) were calculated and plotted against time (Figure 3 (b)). The flux (J) was established as the slope of the linear portion of the plot (Figure 3(b)). The highest transdermal flux was obtained with control liposomes, i.e. conventional vesicles that are recognized to simply act as penetration enhancer and not as true carriers (*Sinico and Fadda 2009*). This result can be due to the unilamellar structure and small size of these vesicles that lead to an increased vesicle/skin interface, thus, favoring interaction with the outermost skin layer followed by the vesicle fusion, a consequent mixing of liposomal bilayers with intercellular skin lipids, and a fast release of the entrapped drug. This, free from the carrier, can permeate rapidly through the disordered and fluidized intercellular skin lipids.

To have an estimation of the main target of the topically applied drug by using PEVs, it is interesting to compare the ratio of DCF accumulated into and permeated through the whole skin, which gives a dimensionless number for the quantification of the Local Accumulation Efficiency (LAC) of the formulations (Figure 3(a)). The highest LAC value was obtained from 10% and 20% Trc-PEVs (LAC =9) that both showed a value 3-fold higher than that of control liposomes (LAC = 3). Overall results (LAC, drug accumulation and permeation values) suggest an important role of PEVs in delivering DCF into the skin where they form a depot from which the drug can be released and diffuse to the deeper tissues until fibroblast, the target of inflammation treatment.

3.3.5. Toxicity studies on 3T3 cells

The toxicity of control liposomes and

Figure 3. (a) Amount of DCF (%) accumulated in stratum corneum (SC), epidermis, dermis and in receptor compartment after 8-h treatment with control liposomes or PEVs; Local Accumulation Capacity (LAC) value was drug accumulated into the skin/drug delivered through the skin ratio. (b) Diffusion of DCF against time from control liposomes or PEVs. J was the transdermal flux (μg/cm^2/h). Data represent the mean ± standard deviation of at least six experimental determinations.

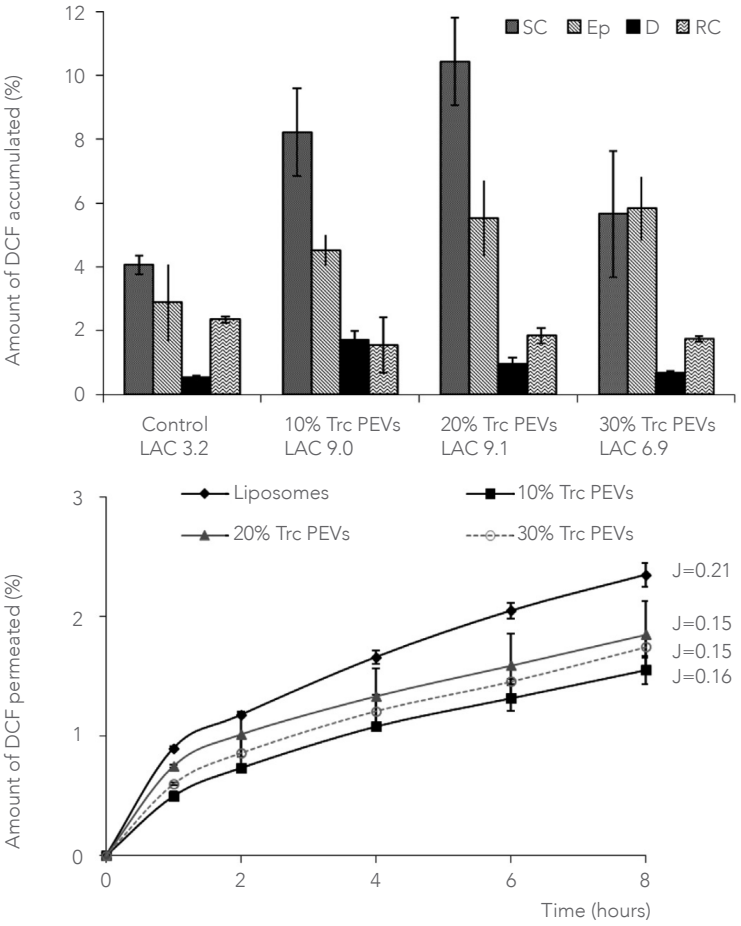

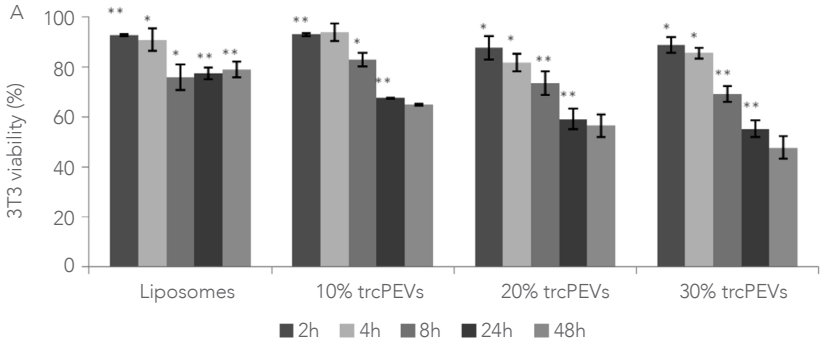

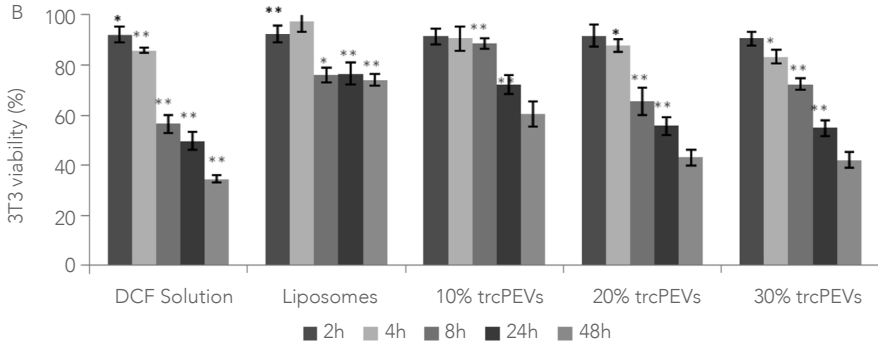

Figure 4. In vitro cytotoxic effect of empty (a) and DCF-loaded liposomes and Trc-PEVs (b) on 3T3 cells at different coincubation times.
*$p < 0.05$, **$p < 0.001$ in comparison with untreated cells (100% viability).

PEVs against mouse 3T3 fibroblasts was evaluated in vitro according to the MTT assay (which measures levels of metabolically active mitochondrial dehydrogenase enzymes). Survival of 3T3 fibroblast was assayed in vitro after incubation with empty and DCF-loaded control liposomes and PEVs at different incubation time (2-4-8-24-48 h). As shown in Figure 4(a), all empty vesicles (control liposomes and PEVs) did not show any significant cytotoxic activity in the first 4 h of incubation (less than 20% mortality) compared to untreated control cells (100% viability). At higher incubation times (8, 24, 48 h), toxicity of control liposomes remained almost constant (~24% mortality) whereas using PEVs especially 20 and 30% Trc-PEVs, viability was reduced. Figure 4(b) shows results of the toxicity study of DCF-loaded vesicles compared to DCF free solution. At 2 and 4 h exposition time, both vesicles and solution did not show any important toxicity (less than 20% mortality).

DCF solution had the highest citotoxicity in particular from 8 h (44% mortality) to 48 h (66% mortality), while in the same period, DCF-loading control liposomes and 10% PEVs significantly improved cell viability, demonstrating a toxicity similar to that of the corresponding empty vesicles. On the contrary, from 8 h exposition time, 20% and 30% Trc-PEVs showed a higher toxic effect, which further increased at 24–48 h. However, it is important to highlight that DCF loaded vesicles were always less toxic than the control solution at the same exposition time and, consequently, results demonstrated that vesicles are able to reduce drug toxicity. Moreover, up to 48 h, DCF control liposomes and 10% Trc-PEVs showed the same statistical cell mortality value of the corresponding empty vesicles (26 and 44% mortality, respectively), whereas using DCF loaded 20% and 30% Trc-PEVs the mortality slightly increased at 24 h and especially at 48 h, probably due to the simultaneous presence of the drug and Trc at higher concentrations (>10%).

3.3.6. Uptake studies on 3T3 cells

Vesicle uptake by 3T3 fibroblasts was investigated using double fluorescently labeled vesicles, which were loaded with a membrane marker (Rho-PE) and a hydrophilic fluorescent probe (CF). CF was chosen as marker of the liposome content since it is a membrane impermeable probe especially used for investigating membrane integrity and permeability (*Lee et al. 1998; Manconi et al. 2007*). When the cells reached a confluence, they were incubated for 2, 4 and 8 h with the double fluorescently labeled vesicles, used at the same concentration tested for toxicity studies (50 µl of formulation in 500 µl of medium), and imaged immediately by fluorescence microscopy after replacing the medium with fresh particle-free medium in combination with the Hoechst 33258, a blue fluorescent dye used for counterstaining the nucleus. Both control liposomes and PEVs were internalized by the 3T3 living cells as confirmed by the appearance of intense intracellular fluorescence after 2 h of coincubation. Cells incubated with control liposomes, 10% and 30% Trc PEVs displayed a comparable intracellular fluorescence pattern: a punctate fluorescence of the Rho-PE in all cytoplasm and a diffuse fluorescence of CF mostly localized in the perinuclear area were detected (Figure 5), suggesting a vesicle internalization by Golgi-endosomal compartment followed by release of the hydrophilic probe.

In particular, in the case of 3T3 living cells coincubated with 10% Trc PEVs intracellular Rho-PE-red fluorescence appears at all tested time points (especially at 4 and 8 h) and show a punctate pattern localized in the perinuclear area (data not shown). CF shows a diffuse green fluorescence very similar at all exposition time. As an example, Figure 5 shows 30% Trc PEVs-treated cells, where the highest liposomal internalization was observed at all time but, simultaneously, the accumulation of the Rho-PE fluorescence was quite different from cell to cell. Indeed, some cells were full of cytoplasmic red fluorescence while other ones appeared almost empty, thus,

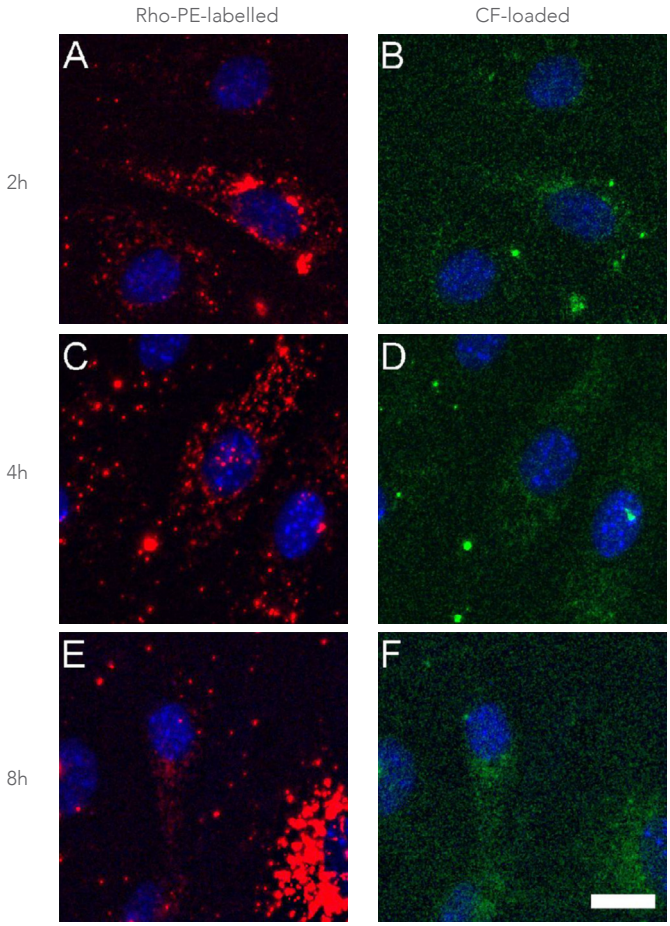

Figure 5. Images of 3T3 fibroblasts incubated for 2, 4 and 8 h with Rho-PE labeled and CF loaded 30% Trc-PEVs. The localization and intensity of dyes are displayed in red for Rho-PE , in green for CF , and in bleu for Hoechst. Bar = 20 µm.

suggesting a great variability in cell uptake (Figure 5 C). Conversely, the fluorescence pattern in cells incubated with 20% Trc PEVs (Figure 6) was very different. Indeed, these vesicles were strongly bound together to form a gel-like supramolecular system making fluorescent aggregates that, in spite of the extensive washing with the culture medium, stayed attached to the plasma membrane surface. In composite color images these vesicle aggregates can be clearly identified as very fluorescent yellow bodies resulting from the co-localization of the two probes (Figure. 6b and c). Therefore, images suggest that these large aggregates could not be readily taken up by the cells because of their size but they stayed intact adhering on the cell surface. However, focusing on cell nucleus, a diffuse red and green perinuclear fluorescence can be detected (Figure 6d and f), thus confirming that a partial internalization had taken place also with 20%Trc PEVs, as established by fluorescence data (Figure 7a and b). The increased cytoplasmic uptake of 10% and 30% Trc PEVs was confirmed by the results of quantification of intracellular Rho-PE fluorescence intensity. A statistical significant increase of red fluorescent intensity was observed in these formulations when compared to control liposomes (Figure 7a). The variability in cell uptake of 30% Trc PEVs was also confirmed by the SD values. The higher Rho-PE fluorescence intensity in 10% and 30% Trc PEVs was not accompanied by a proportional fluorescence intensity of CF. In fact, Trc-PEVs treated cells displayed the same CF content in comparison with control liposomes, probably because CF loading capacity of Trc-PEVs decreased as Trc concentration increased. Indeed, CF entrapment efficiency diminished according the following rank: liposomes (47 ± 6%) > 10%Trc PEVs (39 ± 5%) > 20% Trc PEVs (34 ± 4%)> 30% Trc PEVs (29 ± 5%). Finally, 20% Trc-PEVs showed Rho-PE and CF fluorescence values equal o minor than those of control liposomes due to the formation of vesicle aggregates on the membrane surface of the cells.

Figure 6. Overlay of phase contrast and fluorescence image of cells exposed to 30% Trc-PEVs (a) and 20% Trc-PEVs (b). Rho-PE and CF loaded 20% Trc-PEVs made fluorescent aggregates that appear as fluorescent yellow spots attached to the plasma membrane in the composite color image (c). Images of Rho-PE (d), CF (e) and merged (f) fluorescence of a cell focused on the nucleus. Bar = 20 μm.

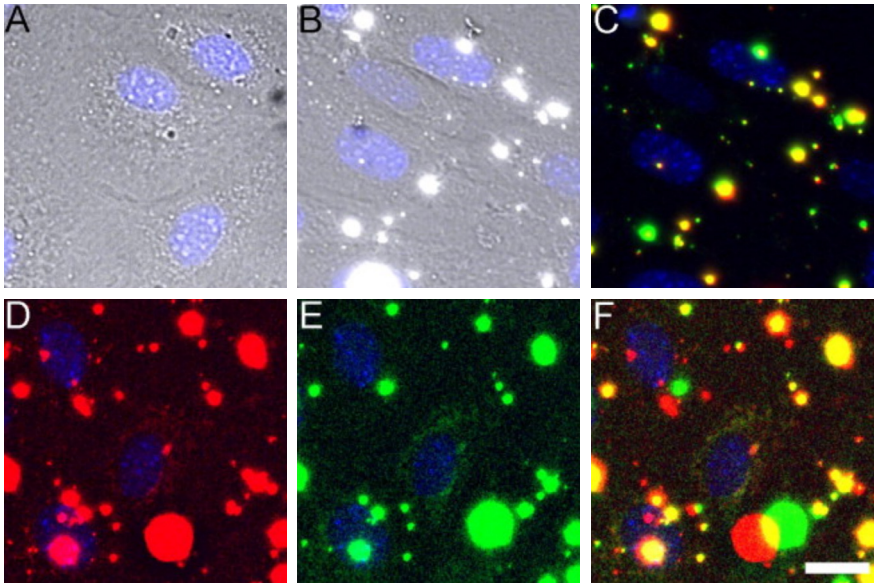

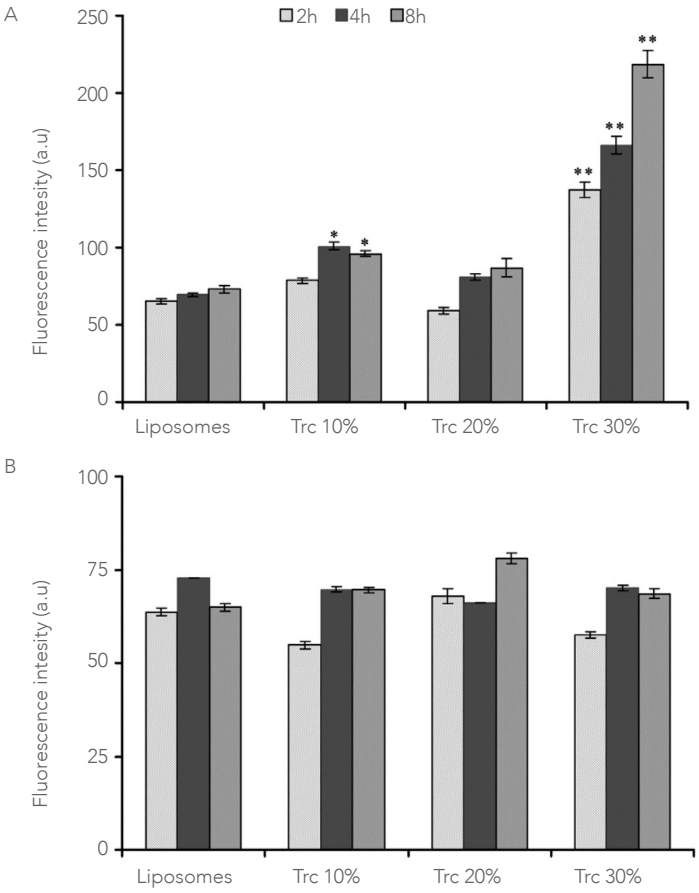

Figure 7. Rho-PE (a) and CF (b) fluorescence values inside the cells. Number of measurements: n = 390, bars represent means ± standard deviation.

3.4. Conclusion

This work has shown that the studied concentrated and densely packed Trc containing vesicles are good candidates for topical drug delivery. Indeed, these new nanocarriers are able to form a gel-like interconnected vesicular dispersion that is characterized of a viscosity higher than that of water. Moreover, as the formulation is topically applied, the expanse structure of the system evolves to single, small vesicles that carry the drug into and through the skin favoring its cutaneous deposition and, thus, interaction with fibroblasts. In vitro study with cells, performed by using vesicles co-labeled with lipophilic and hydrophilic markers, has also proved that these high lipids concentrated PEVs are capable of being internalized by the 3T3 fibroblasts. The vesicular carrier has also been demonstrated to reduce the in vitro drug toxicity. Therefore, the outcomes of the present investigation suggest these new transcutol containing close packed vesicles are good candidates for improving DCF dermal delivery.

4. EFFECT OF DICLOFENAC AND GLYCOL INTERCALATION ON STRUCTURAL ASSEMBLY OF PHOSPHOLIPID LAMELLAR VESICLES

Published in International Journal of Pharmaceutics 456 (1), 1-9, 2013

4.1. Introduction

Several studies have been carried out to explore the interactions of drug or other components with lamellar vesicles and their effects on the bilayer structure (*Kranenburg, Vlaar, and Smit 2004; Pignatello, Intravaia, and Puglisi 2006; Rosser, Lu, and Dea 1999*). Any small molecules might cause bilayer packing alteration and among these chemicals, aliphatic alcohols are the best known and studied (*Adachi et al. 1995; Kranenburg et al. 2004; Löbbecke and Cevc 1995*). In particular, a large number of studies have been focused on ethanol effects in phospholipid vesicles (*Celia et al. 2009; Touitou et al. 2000*). Results suggested that ethanol plays a significant role in the arrangements of phospholipids on the bilayer, changing the acyl chain orientation inside the lamellar structure and usually forming an interdigitated structure (*Adachi et al. 1995; Komatsu and Okada 1995*). Thanks to this, ethanol forms soft and fluid lamellar vesicles able to improve skin delivery of several drugs. Alternatively to ethanol, others water miscible cosolvents such as isopropyl alcohol and propylene glycol (PG), have been used as additive of vesicle bilayer to make innovative phospholipid vesicles able to facilitate drug delivery, especially skin delivery (*Caddeo et al. 2012; Chessa et al. 2011; Elmoslemany et al. 2012; Elsayed et al. 2007; Manconi, Caddeo, et al. 2011*). However, the interactions involved among drug, water, cosolvent and phospholipid and the possible rearrangements that take place into bilayer were not deeply investigated. We recently reported the effect of diethylene glycol monoethyl ether (Transcutol®, Trc) and propylene glycol on self-assembling and rheological properties of phosphatidylcholine lamellar vesicles and we found that 10–20% of glycols allowed the formation of vesicles with the more suitable and stable features (*Manconi et al. 2012*).

Here, the interactions between hydrogenated phosphatidylcholine bilayer vesicles and the two glycols, differing in their structure, have been extensively studied. In particular, the effective glycol ability

to perturb phospholipid vesicle bilayer and the simultaneous effect of diclofenac sodium salt, were evaluated. This potent antinflammatory drug is commercially available in semisolid preparations for topical application (*Escribano et al. 2003*). In this work it was used as model drug able to perturb phospholipid bilayer structure, thanks to its amphiphilic properties (*Schreier, Malheiros, and de Paula 2000*) (*Lopes et al. 2004; Manconi et al. 2009; Manconi, Caddeo, et al. 2011*).

The aim of the current study was to improve the knowledge of drug–glycol–phospholipid-interactions and their effects in lamellar vesicle aptitude as topical carrier. The simultaneous addition of diclofenac sodium salt and a hydrophilic glycol (Trc or PG) to phospholipid dispersion led to the formation of a vesicle structure with a complex intervesicle architecture. These important structural rearrangements were disclosed by a change on physical state from liquid to high viscous liquid or soft-solid like. The effects, at molecular level, have been monitored by combining the information obtained by differential scanning calorimetry (DSC), small- and wide-angle diffraction signals (SAXS) and rheology studies. These techniques permitted to build a detailed picture of intra- and inter-vesicle assembly.

4.2. Materials and methods

4.2.1. Materials

Hydrogenated soy phosphatidylcholine (Phospholipon® 90H, P90H) was kindly supplied by AVG S.r.l. (Milan, Italy) and Lipoid GmbH (Ludwigshafen, Germany). Diethylene glycol monoethyl ether (Transcutol® P, Trc) was kindly provided by Gattefossè (Saint Priest, France). Phosphate buffer solution (PBS, pH 7) was purchased from Carlo Erba Reagents (Milan, Italy). Diclofenac sodium salt (DCF-Na), cholesterol (Chol), and propylene glycol (PG) were purchased from Sigma–Aldrich (Milan, Italy).

4.2.2. Vesicle preparation

Liposomes were prepared by using P90H

(60 mg/ml), Chol (2 mg/ml), DCFNa (5 and 10 mg/ml) and PBS. PEVs were obtained using the same lipid phase (P90H, Chol), DCFNa (5 and 10.mg/ml) and a mixture of Trc/PBS or PG/PBS (5, 10, 20%, v/v) as water phase (Table 1). All components were weighted in a glass flask, hydrated with the water phase, and finally sonicated (5 s on and 2 s off, 30 cycles; 14 μm of probe amplitude) with a high intensity ultrasonic disintegrator (Soniprep 150, MSE Crowley, London, United Kingdom) (Madrigal-Carballo et al. 2008; Manconi et al. 2003). Each formulation was purified from the non-encapsulated drug by dialysis. Samples were loaded into dialysis tubing (Spectra/Por® membranes: 12–14 kDa MW cut-off, 3 nm pore size; Spectrum Laboratories Inc., DG Breda, The Netherlands) and dialysed against PBS (liposomes) or appropriate glycol/PBS (PEVs) mixtures for 2 h at 5 °C, to allow the dissolution and removal of the non-encapsulated drug and non-aggregated phospolipids.

4.2.3. Vesicle characterization

Vesicle formation and morphology were assessed by cryo transmission electron microscopy (cryo-TEM) analysis. A thin aqueous film was formed by placing a 5 μl sample drop on a glow-discharged holey carbon grid and then blotting the grid against filter paper. The resulting thin films spanning the grid holes were vitrified by plunging the grid (kept at 100% humidity and room temperature) into ethane, which was maintained at its melting point with liquid nitrogen, using a Vitrobot (FEI Company, Eindhoven, The Netherlands). The vitreous films were transferred to a Tecnai F20 TEM (FEI Company) using a Gatan cryotransfer (Gatan, Pleasanton, CA), and the samples were observed in a low dose mode. Images were acquired at 200 kV at a temperature between 170 and 175 C, using low-dose imaging conditions not exceeding 20 e−/Å2, with a CCD Eagle camera (FEI Company).

The average diameter and polydispersity index (PI), as a measure of the width of the size distribution of the samples,

were determined by Photon Correlation Spectroscopy using a Zetasizer nano-ZS (Malvern Instruments, Worcestershire United Kingdom). Samples were back-scattered by a helium–neon laser (633 nm) at an angle of 173° and a constant temperature of 25 °C. Zeta potential was estimated using the Zetasizer nano-ZS by means of the M3-PALS (Mixed Mode Measurement-Phase Analysis Light Scattering) technique, which measures the particle electrophoretic mobility in a thermostated cell. Each sample (10 µl) was diluted with 10 ml of PBS or the appropriate glycol/PBS mixture before analysis. Drug entrapment efficiency (EE%), expressed as the percentage of the drug amount after dialysis versus that initially used, was determined by high performance liquid chromatography (HPLC) after disruption of vesicles with methanol (1:1000 dilution). Diclofenac sodium content was quantified at 227 nm using a chromatograph Alliance 2690 (Waters, Milan, Italy) equipped with a column Symmetry C18 (3.5 mm, 4.6 100 mm, Waters). The mobile phase was a mixture of water/acetonitrile (30/70, v/v), delivered at a flow rate of 0.5 ml/min (6).

The lipid content of dispersions was determined by the Stewart (1980) (Stewart 1980) assay. Briefly, an aliquot of liposomes or PEV dispersions was added to a biphasic mixture of aqueous ammonium ferrithiocyanate solution (0.1 N) and chloroform. The concentration of P90H was obtained by measuring absorbance at 485 nm of the organic solution. The aggregation efficiency (AE%) represented the effective amount of aggregated phospholipids (after dialysis) expressed as the percentage of the initially used amount.

4.2.4. Vesicle stability

The vesicle stability was assessed by monitoring the vesicle average size and zeta potential over 90 days at 4 ± 1 °C. Drug release from the vesicles during the storage was evaluated by measuring the liposomes encapsulation efficiency over 90 days.

Table 1. Acronyms, composition and physical state of liposomes and PEVs. Vesicles appeared as liquid, high viscous liquid (HV liquid) or soft solid.

Sample	P90H (mg/ml)	Chol (mg/ml)	DCF_{Na} (mg/ml)	Trc (% v/v)	PG (% v/v)	PBS (% v/v)	Physical state
Empty liposomes	60	2	0	0	0	100	Liquid
5DCF liposomes	60	2	5	0	0	100	Liquid
5DCF 5Trc-PEVs	60	2	5	5	0	95	Liquid
5DCF 10Trc-PEVs	60	2	5	10	0	90	HV Liquid
5DCF 20Trc-PEVs	60	2	5	20	0	80	Soft solid
5DCF 5PG-PEVs	60	2	5	0	5	95	Liquid
5DCF 10PG-PEVs	60	2	5	0	10	90	HV Liquid
5DCF 20PG-PEVs	60	2	5	0	20	80	Soft solid
10DCF liposomes	60	2	10	0	0	100	Liquid
10DCF 5Trc-PEVs	60	2	10	5	0	95	HV Liquid
10DCF 10Trc-PEVs	60	2	10	10	0	90	Soft solid
10DCF 20Trc-PEVs	60	2	10	20	0	80	Soft solid
10DCF 5PG-PEVs	60	2	10	0	5	95	HV Liquid
10DCF 10PG-PEVs	60	2	10	0	10	90	HV Liquid
10DCF 20PG-PEVs	60	2	10	0	10	90	Soft solid

4.2.5. Differential scanning calorimetry analysis

DSC studies were performed using a DSC Mettler Toledo model 821e (Mettler Toledo International Inc., Barcelona, Spain). The samples were scanned in a sealed aluminum pans under nitrogen atmosphere. DSC thermograms were scanned in the first heating run at a constant rate of 10 °C/min and a temperature range of 0–80 °C.

4.2.6. X-ray diffraction

Vesicle structure of liposomes and PEVs was probed by small- and wide-angle X-ray scattering (SWAXS). SAXS and WAXS patterns were recorded simultaneously using two linear, one-dimensional, position-sensitive detectors (PSD 50 M; Hecus X-Ray Systems) containing 1024 channels of width 54.0 μm. Cu Kα radiation of wavelength 1.542 Å was provided by a GeniX X-ray generator, operating at 50 kV and 1 mA.

The working q-range were 0.003–0.6 Å−1 for SAXS and 1.3–1.9 Å−1 for WAXS, where $q = (4\pi \sin\theta)/\lambda$ is the modulus of the scattering wave vector, θ the scattering angle and λ the wavelength. All scattering curves, recorded at 25 °C, were reproduced twice with subsequent calculation of the electron distance distribution, and yielded identical results. For the figures, a representative curve was selected, plotting the scattering intensity (I) as a function of the scattering vector (q). The calibration of the q-scale was performed by measuring silver behenate in the SAXS range and p-bromo-benzoic-acid in the WAXS range.

SAXS patterns were analyzed in terms of a global model using the program GAP (Global Analysis Program) developed by Pabst (Pabst et al. 2000, 2003). The analysis technique models the full q-range in the SAXS regime, including Bragg peaks and diffuse scattering. By this procedure, relevant structural parameters, as well as the distribution of electron density in the polar and apolar regions of membranes, were obtained. The GAP allows fitting the SAXS pattern of bilayer-based structures,

i.e. vesicles and lamellar phases. From the analysis, the membrane thickness was obtained through the definition dB = 2 (zH + 2σH). zH and σH, obtained from SAXS curve fitting with GAP, represent the head group amplitude and its distance to the bilayer center the methyl terminus or lipid half extend respectively.

4.2.7. Rheological studies

Rheological measurements were carried out at 25 ± 1 °C, using a Kinexus rotational rheometer (Malvern Instruments, Worcestershire, United Kingdom) equipped with data acquisition and elaboration software rSpace; a cone-plate geometry (CP1/60) was used. Before each analysis, a thin layer of silicon oil (Dimethicone, RFE/Ph. Eur.) was laid on the free surface of the sample to prevent water evaporation. Frequency sweep tests were performed in the range 0.01–10 Hz and a shear stress of 0.1 Pa was used. Mechanical spectra of the storage (G′) and loss (G″) moduli were registered in the above mentioned frequency range and G′ at 1 Hz was used to characterize the viscoelastic properties of the different dispersions. Before frequency sweep experiments, amplitude sweep experiments were carried out for each sample to determine the linear viscoelastic region where the values of the moduli are independent by the applied deformation. Steady shear experiments were performed in the range 0.01–20 Pa. Viscosity at 1 s−1 was used to characterize the flow properties of different dispersions. All measurements were carried out in triplicate.

4.2.8. Statistical analysis of data

Data analysis was carried out with the software package R, version 2.10.1. Results are expressed as the mean ± standard deviation. Multiple comparisons of means (Tukey's test) were used to substantiate statistical differences between groups, while Student's t-test was used for comparison between two samples. Significance was tested using at least 0.05 level of probability (p).

4.3. Results and discussion

4.3.1. Liposome and PEV preparation and characterization

In the present work Trc or PG were mixed in the water phase at different concentrations (5, 10, 20%, v/v) to obtain innovative P90H phospholipid vesicles termed PEVs (penetration enhancer containing vesicles) to distinguish them from conventional liposomes. DCFNa, widely used for the treatment of local and chronic inflammatory disease, was used as a model drug at two different concentrations (5 and 10 mg/ml) in order to investigate the ability of this amphiphilic molecule to interact with phospholipids and to cause modifications of the vesicles structure (*Lopes et al. 2004; Tavano, Muzzalupo, Trombino, et al. 2010*). In order to carry out an appropriate comparison, empty and DCFNa loaded liposomes were also prepared and characterized. Acronyms, composition and physical state of samples are summarized in Table 1. At visual inspection, important differences on sample physical state were evident: liposomes were liquid while vesicles containing low glycol concentrations appeared highly viscous liquid probably due to different and concomitant effects such as the use of a hydrogenated phospholipid at high concentration and the simultaneous presence of drug and glycols. Finally, 5-10DCF 20glycol-PEVs and 10DCF 10Trc-PEVs, were soft-solid like indicating a change on packing assembly and/or vesicle interactions. A similar physical state was not observed in formulations previously prepared using not-hydrogenated phosphatidylcholine, Transcutol or propylene glycol and diclofenac sodium salt, these vesicles appeared viscous instead (*Manconi et al. 2009, 2012; Manconi, Caddeo, et al. 2011*).

Cryo-TEM microscopy was used to observe structure and morphology of liposomes and PEVs. It is a valid imaging technique able to ensure a truthful sample observation because the sample remains as native as possible, without the aid of staining and drying process. Empty and

Figure 1. Cryo-TEM micrographs of 5DCF control liposomes (A), 5DCF 5PG-PEVs (B), 10DCF 10PG-PEVs (C), and 10DCF 20Trc-PEVs (D).

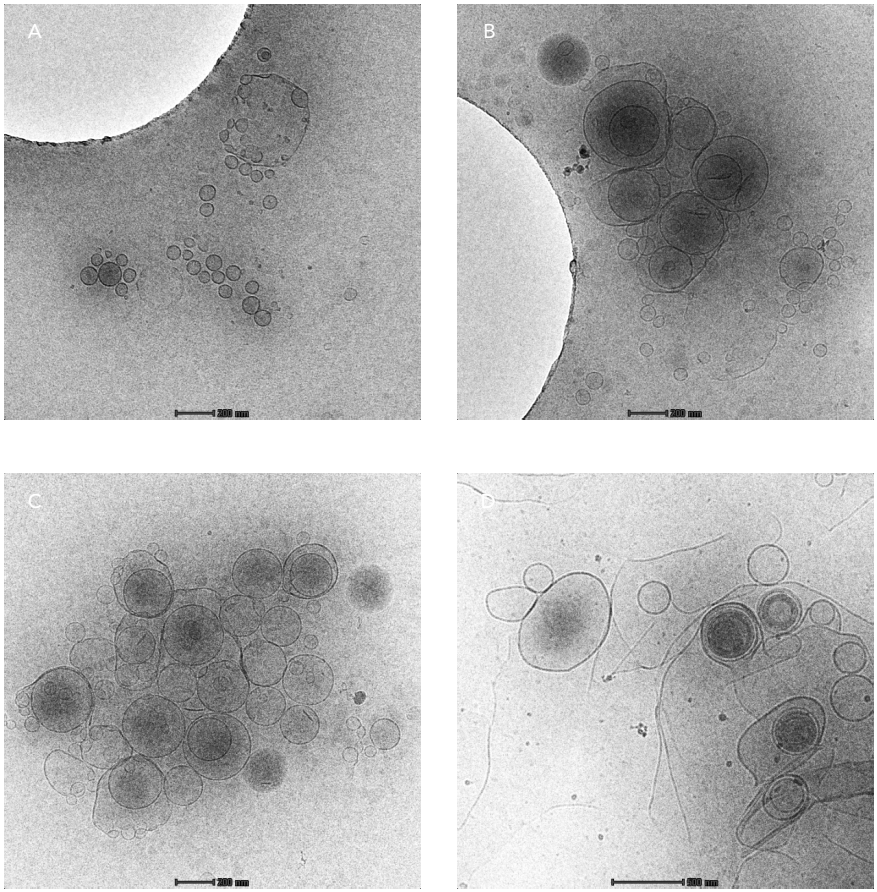

DCFNa loaded liposomes were mostly unilamellar with a spherical shape (Figure 1A). PEVs exhibited a peculiar behavior by forming mainly unilamellar vesicles that were closely packed (Figure 1B and C), especially 20glycol-PEVs, where bilayers forming bridges between the vesicles were visualized (Figure 1D). Empty liposomes had a mean diameter around 160 nm, whereas the addition of DCFNa (5 or 10 mg/ml) allowed a reduction of vesicle size to ~95 nm ($p < 0.01$) (Table 2). Vesicle size reduction is commonly observed after incorporation of DCFNa, possibly because its amphiphilic properties is able to self-associate and to fit within the bilayer causing (at high concentration) disruption and solubilization similar to that induced by detergents (Lopes et al. 2004; Schreier et al. 2000; Schütze and Müller-Goymann 1998). Zeta potential of empty liposomes was slightly negative (−6 mV) because at pH 7.0, phosphate groups of phosphatidylcholine were charged and oriented on liposome external surface (Abramović et al. 2008). Zeta potential of DCFNa containing liposomes was more negative (−29 mV) suggesting the adsorption of the negative charged molecules of drug on the bilayer surface. 5-10DCF 5-10glycol-PEVs showed a mean diameter ranging from 80 to 124 nm, smaller ($p < 0.05$) than that of empty liposomes, except for 10DCF 10Trc-PEVs. DCFNa loaded 20glycol-PEVs were the largest vesicles ($p < 0.05$) and it was noted that mean diameter increased as the concentration of glycols increased, with the exception of 5DCF 5PG-PEVs and 5DCF 10PG-PEVs that showed almost the same diameter ($p > 0.05$). The simultaneous presence of drug and glycols in PEVs led to a lower negative zeta potential than that of DCFNa loaded liposomes (~−28 mV) as the glycol concentrations increased.

The smallest vesicles of tested samples were 10DCF 5PG-PEVs (80 nm) probably because this concentration of drug and PG allowed the best phospholipid packing. These vesicles exhibited as well an adequate negative zeta potential (−17

Table 2. Mean diameter, polydispersity index (PI), zeta potential (ZP), encapsulation efficiency (EE%), and aggregation efficiency (AE%) of P90H liposomes and PEVs. Mean values ± standard deviation are reported (n = 6).

Sample	DCF_{Na} (mg/ml)	Size (nm)	PI	ZP (mV)	EE (%)	AE (%)
Empty liposomes	0	160±8	0.31±0.04	-6±2		98
5DCF liposomes	5	97±7	0.31±0.01	-29±4	58±3	95
5DCF 5Trc-PEVs	5	105±4	0.28±0.09	-8±2	61±6	96
5DCF 10Trc-PEVs	5	119±9	0.31±0.02	-1±3	60±2	99
5DCF 20Trc-PEVs	5	178±6	0.32±0.01	-1±2	57±4	86
5DCF 5PG-PEVs	5	111±8	0.31±0.04	-6±4	61±1	98
5DCF 10PG-PEVs	5	100±4	0.24±0.06	-3±2	54±3	99
5DCF 20PG-PEVs	5	159±6	0.26±0.04	-2±3	58±3	91
10DCF liposomes	10	94±4	0.32±0.02	-28±5	53±5	99
10DCF 5Trc-PEVs	10	124±5	0.24±0.06	-16±4	50±6	99
10DCF 10Trc-PEVs	10	157±8	0.32±0.03	-5±3	46±2	96
10DCF 20Trc-PEVs	10	208±9	0.33±0.02	-3±4	51±4	92
10DCF 5PG-PEVs	10	80±13	0.26±0.06	-17±5	47±5	92
10DCF 10PG-PEVs	10	109±13	0.25±0.02	-13±4	45±4	95
10DCF 20PG-PEVs	10	193±16	0.30±0.07	-2±2	50±4	89

mV) able to assure a good stability. The smallest size among Trc-PEVs was obtained whit 5DCF 5Trc-PEVs (105 nm) which however showed a slightly negative zeta potential insufficient to ensure a good stability of the dispersions. Then, Trc-PEVs reached the best packing and consequently smaller vesicle size with 5 mg/ml of DCFNa while PG-PEVs allowed the smallest vesicle size with 10 mg/ml of DCFNa showing a superior ability of phospholipid/PG mixture to provide a suitable carrier able to entrap the highest amount of drug in the smallest vesicles.

Encapsulation efficiency was quite the same for all the tested formulations and was slightly higher for 5DCF PEVs than that of corresponding 10DCF PEVs probably because in the latter case the drug amount used was 2-fold higher, thus reaching vesicle saturation. Actually, 10DCF PEVs encapsulated an higher drug amount (~4.8 mg/ml) than 5DCF vesicles (~3 mg/ml). Whereas, the glycol structure and concentration, did not affect the encapsulation efficiency.

Aggregation efficiency, expressed as the percentage of phosphatidylcholine after dialysis with respect to the initial amount, seems to be affected by glycol concentration but not by drug concentration. Aggregation efficiency was statistically similar for all 5-10DCF 5-10glycol-PEVs (91–99%) and slightly decreased only for 5-10DCF 20glycol-PEVs; probably this amount of glycol, which is able to decrease the dielectric constant of the medium with respect of water, partially solubilized a small fraction of phospholipids that remain in the free form within the dispersion.

4.3.2. Stability during storage of liposomes and PEVs

Physico-chemical features (average size, zeta potential, and drug leakage) of the tested formulations were checked during 90 days to evaluate the system stability. Mean diameter of 20Trc-PEVs and 20PG-PEVs (Figure 2A and C) at 60 or 90 days strongly increased, especially 5DCF 20PG-PEVs that exceed 1 μm after 60

days whereas 5-10DCF 20Trc-PEVs and 10DCF 20PG-PEVs reached a maximum diameter of 800 nm. 5-10glycol-PEVs were almost stable and their size did not exceed 300 nm.

During the storage all the tested samples released increasing amounts of drug (Fig. 2B and D). The lose of drug was more evident in 20glycol-PEVs that were in soft solid-like tate; this sample also showed a strong increase in size due to vesicle aggregation and fusion. Aggregation phenomena of vesicle dispersions is controlled by a balance of attraction forces and electrostatic repulsion forces. In this case, the low surface charge of 20glycol-PEVs (±5 mV) was unable to ensure an electrostatic repulsion enough to prevent vesicle aggregation and fusion, thus promoting drug release during storage.

4.3.3. DSC studies

DSC is a sensitive thermodynamic technique which has been extensively used to evaluate thermotropic phase of phospholipid vesicles and their transition from gel to liquid-crystalline state (*Thomas and Finnin 2004*). Table 3 reported the transition temperatures obtained for each formulation. Empty liposomes were characterized by a single endothermic peak at 54 ± 0.5 ˚C, characteristic of a cooperative gel to liquid-crystalline main phase transition. Pretransition peak was abolished by the addition of cholesterol and by the presence of free fatty acids and triglycerides in the soy lipid mixture called P90H (MANCONI et al. n.d.). The addition of DCFNa clearly reduced the transition temperature of all tested formulations from ~54 ˚C to ~50 ˚C, probably due to an increase of vesicle curvature (corresponding to a vesicle size reduction) caused by the drug intercalation on bilayer structure, thus modifying its packing (*Feitosa, Barreleiro, and Olofsson 2000*). 5DCF and 10DCF liposomes showed the same transition temperature at 50 ± 0.4 ˚C demonstrating that the drug is able to perturb the bilayer structure regardless of its concentration in the range studied. In PEV formulations the reduction of tem-

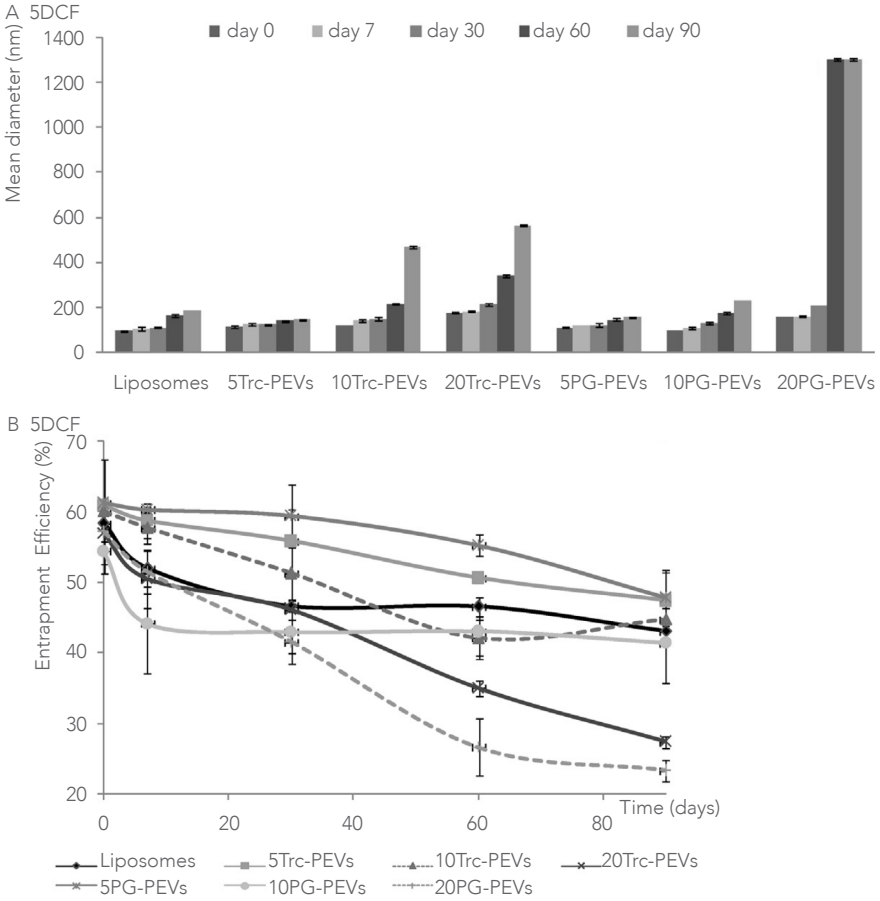
A 5DCF
Mean diameter (nm)
day 0
day 7
day 30
day 60
day 90
1400
1200
1000
800
600
400
200
0
Liposomes
5Trc-PEVs
10Trc-PEVs
20Trc-PEVs
5PG-PEVs
10PG-PEVs
20PG-PEVs
B 5DCF
Entrapment Efficiency (%)
70
60
50
40
30
20
0
20
40
60
80
Time (days)
Liposomes
5Trc-PEVs
10Trc-PEVs
20Trc-PEVs
5PG-PEVs
10PG-PEVs
20PG-PEVs

Figure 2. Mean diameter and DCFNa entrapment efficiency during 90 days of storage. Mean diameter (A) and encapsulation efficiency (B) of 5 mg/ml DCFNa loaded vesicles. Mean diameter (C) and encapsulation efficiency (D) of 10 mg/ml DCFNa loaded liposomes and different PEVs. Mean values ± standard deviation are reported (n = 6).

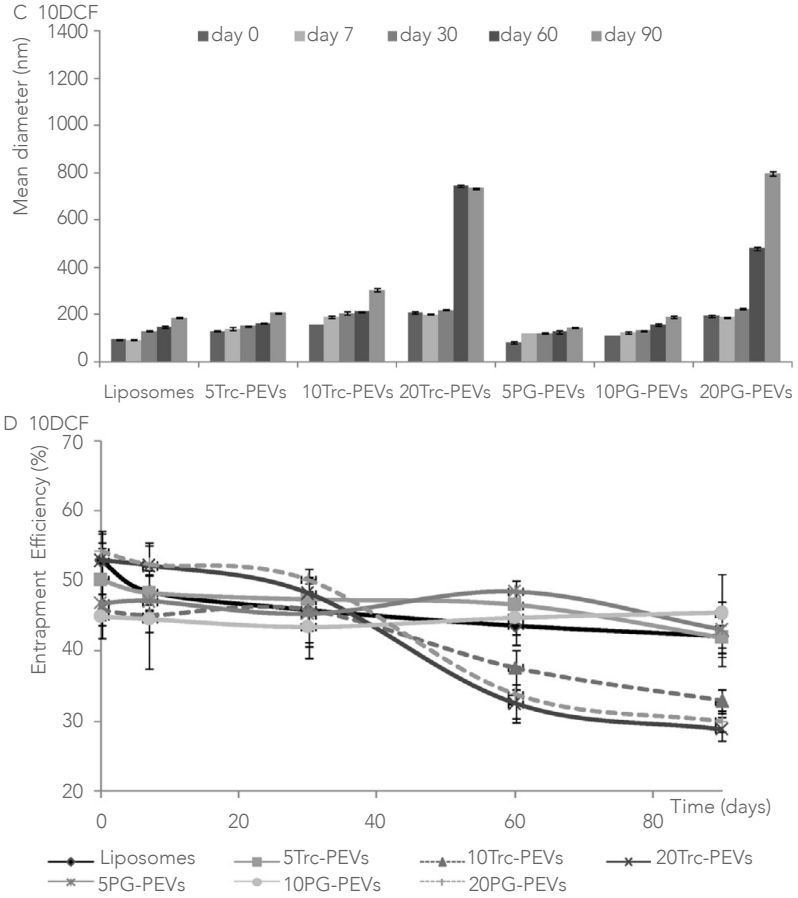

Sample	T_t (°C)	structure	d (Å)	Z_h (Å)	σ_h (Å)	d_b (Å)	Dwaxs (Å)
Empty liposomes	54±0.5	ULV	nd	20.6±0.5	2.8±0.3	58.8±3	4.2Pβ'
5DCF liposomes	50±0.4	ULV	nd	17.3±0.3	2.2±0.2	53.0±3	4.2Pβ'
5DCF 5Trc-PEVs	50±0.4	ULV	nd	16.5±0.5	1.9±0.3	41.0±1	4.2Pβ'
5DCF 10Trc-PEVs	50±0.4	ULV	nd	15.8±0.6	1.4±0.4	37.0±2	4.2Pβ'
5DCF 20Trc-PEVs	51±0.3	-	-	-	-	-	-
5DCF 5PG-PEVs	51±0.4	ULV	nd	16.4±0.3	1.9±0.5	40.8±2	4.2Pβ'
5DCF 10PG-PEVs	49±0.5	ULV	nd	16.4±0.5	1.2±0.4	37.6±1	4.2Pβ'
5DCF 20PG-PEVs	51±0.3	ULV	nd	16.5±0.4	2.1±0.3	41.8±2	4.2Pβ'
10DCF liposomes	50±0.4	ULV	nd	15.8±0.3	1.4±0.3	37.8±2	4.2Pβ'
10DCF 5Trc-PEVs	49±0.5	ULV	nd	15.6±0.4	1.4±0.2	37.0±1	4.2Pβ'
10DCF 10Trc-PEVs	49±0.3	OLV	60±2	15.5±0.4	1.1±0.3	36.0±1	4.2Pβ'
10DCF 20Trc-PEVs	50±0.3	-	-	-	-	-	-
10DCF 5PG-PEVs	50±0.4	ULV	nd	15.2±0.3	1.7±0.2	38.6±2	4.2Pβ'
10DCF 10PG-PEVs	49±0.4	ULV	nd	15.9±0.5	1.4±0.3	37.8±2	4.2Pβ'
10DCF 20PG-PEVs	50±0.5	OLV	50±0.4	15.8±0.3	1.3±0.2	36.8±1	4.2Pβ'

Table 3. Main transition temperature (Tt) of P90H liposomes and glycol-PEVs obtained by DSC investigation. Unilamellar (ULV) or oligolamellar (OLV) vesicles, lamellar spacing (d), bilayer thickness (d_B), distance of headgroup from the center of the bilayer or lipid half extent (Z_H), polar head amplitude (σ_h) and WAXS distance calculated from scattering curve of empty and DCFNa-loaded liposomes and glycol-PEVs. Each single value represents the average ± standard deviation of three determinations.

perature transition was slightly dependent on the drug concentration. A low reduction (~1 ˚C) has been observed as the drug concentration increased: 10DCF PEVs showed lower transition temperature than that of the corresponding 5DCF PEVs, probably because the simultaneous drug and glycol intercalation, within the bilayer surface, allowed the formation of an interdigitated bilayer. Glycols slightly altered the transition temperature and the resulting effects depended on their structure and concentration. This phenomenon probably can be due to their presence in the inter-vesicle spaces where led a reduction of the dielectric constant of the medium, thus reducing the charged groups on the interfacial bilayer region and inducing a series of intra- and inter-vesicle transformations (*Rosser et al. 1999; Vierl et al. 1994*)(*Manconi et al. 2012*).

4.3.4. Small- and wide-angle X-ray scattering analysis

The molecular rearrangements that take place in vesicles were confirmed by SWAXS, a useful tool to investigate microscopic change inside phospholipid bilayer that provides detailed information at the molecular level about the influence of external compounds on the lamellar organization of vesicles. WAXS diffraction peak of empty liposomes was asymmetric, diffuse and centered at ~1.52 Å−1 confirming the bilayer state in Lβ′ phase in which the hydrocarbon chains were fully extended and tilted with respect to the bilayer surface. The presence of DCFNa and glycols on phospholipid vesicles led to a more resolved and sharp peak shifted at ≈1.51 Å−1 evidencing the bilayer transition to Pβ′ phase in which the lipid chains were differently organized (Figure 3A).

The incorporation of DCFNa into liposomes led to a marked alteration of lipid layer arrangement and chain packing (Figure 3B and Table 3). SAXS profiles of empty liposomes showed a pure diffuse scattering curve indicating the presence of unilamellar vesicles; the SAXS curves became broadened and low-intense

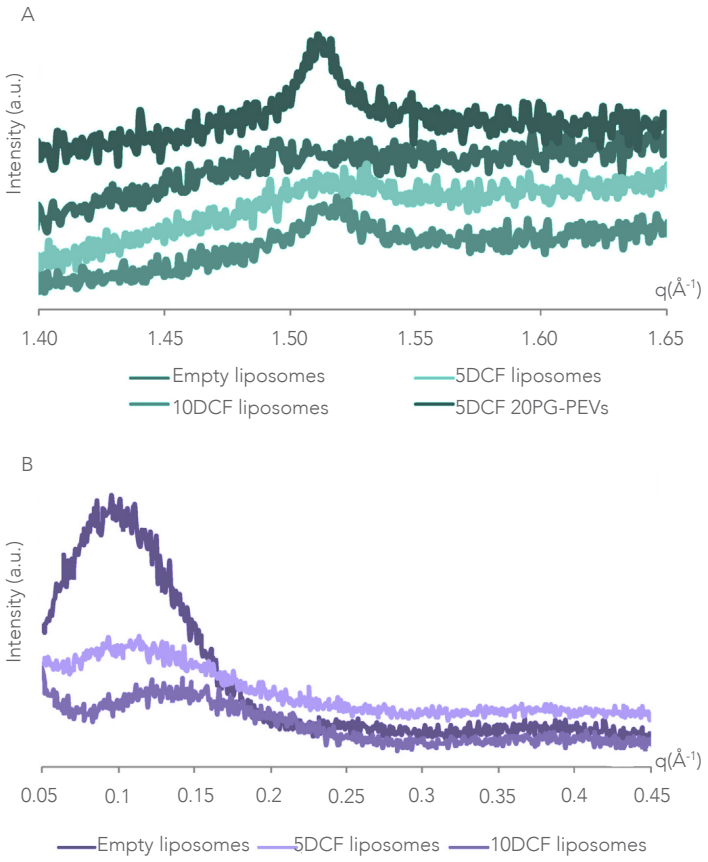
A
Intensity (a.u.)
q(Å-1)
1.40
1.45
1.50
1.55
1.60
1.65
Empty liposomes
5DCF liposomes
10DCF liposomes
5DCF 20PG-PEVs
B
Intensity (a.u.)
q(Å-1)
0.05
0.1
0.15
0.2
0.25
0.3
0.35
0.4
0.45
Empty liposomes
5DCF liposomes
10DCF liposomes

Figure 3. WAXS intensity profile versus the scattering vector modulus (q) reordered from empty liposomes, 5-10DCF liposomes and 5DCF 20PG-PEVs (A); SAXS curves as a function of the scattering vector modulus (q) of empty, 5DCF and 10DCF liposomes, (B); 10DCF liposomes and 10DCF PG-PEVs (C); 10DCF 20Trc-PEVs (D). For the sake of clarity only the more representative curves were reported.

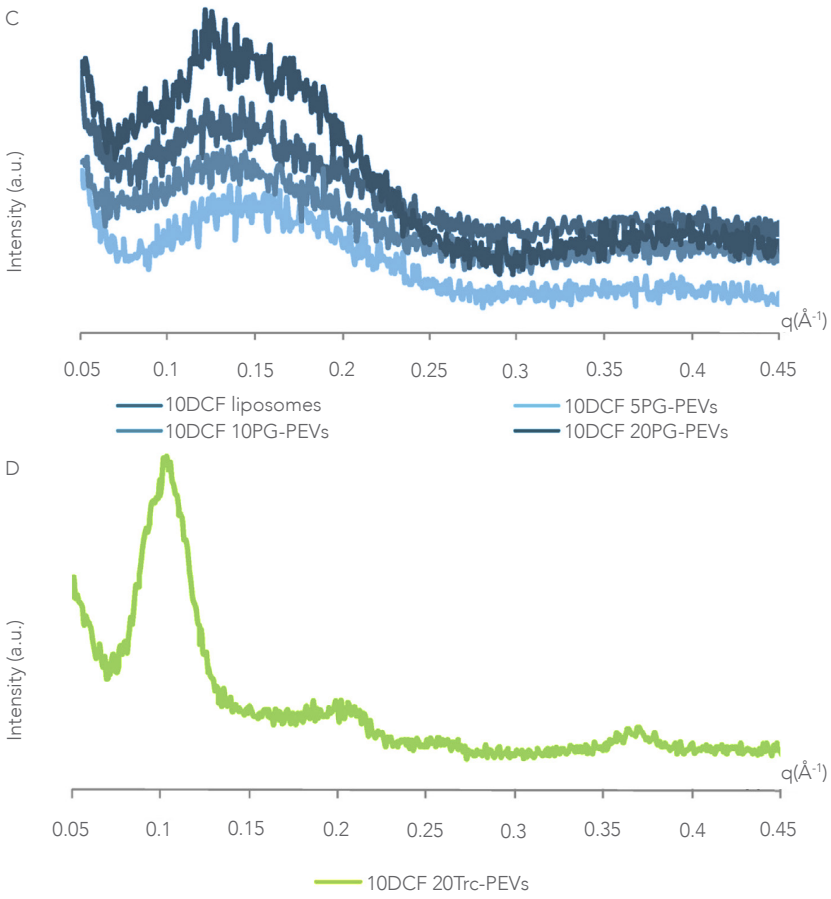

when DCFNa was incorporated, as a result of the strong interaction of the drug with the lipid bilayer. The related bilayer thickness (dB) estimated from Bragg's law decreased from 56.8 ± 0.6 to 53.0 ± 0.6, to 37.8 ± 0.6 Å for empty, 5DCF and 10DCF liposomes respectively, with a simultaneous reduction of polar head amplitude (σh) and lipid half extent (ZH). According to DSC results the drug intercalation between the polar heads of phospholipids allowed the formation of free spaces in the hydrophobic region between achyl chains that moved toward the opposite surface reducing the bilayer thickness (dB 38 Å). The membrane underwent a transformation to interdigitated structure (Pβ') confirmed by lower dB value and sharp WAXS peak.

Also, the association of glycols and DCF-Na, promoted a series of structural changes which led to the bilayer transition to the Pβ' interdigitated phase. These arrangements depending on glycol chemical structure and concentration were evaluated according to modifications on SAXS profile and correlated parameters (Figure 3C and Table 3). Liposomes, 5DCF PEVs (except 5DCF 20Trc-PEVs), 10DCF 5Trc-PEVs and 10DCF 5-10PG-PEVs were always unilamellar presenting a first order diffraction peak centered at ~0.11 Å−1 for 5DCF vesicles and shifted at ~0.14 Å−1 for 10DCF vesicles. The first order peak of 10DCF 10Trc-PEVs and 10DCF 20PG-PEVs appeared at ~0.12 Å−1 and presented a shoulder at ~0.18 Å−1 due to the presence of a different population of multilamellar vesicles. All PEVs were in the interdigitated phase as confirmed by the low bilayer thickness (dB ~ 38 Å) and a WAXS sharp peak. The bilayer thickness reduction was associated to a simultaneous decrease of polar head amplitude (σh) and lipid half width (ZH). As reported previously, Transcutol and DCF-Na interacted together with the polar bilayer surface, producing empty spaces at bilayer midplane, forming an acyl-chain interdigitation and a consequent compression of bilayer thickness and packing rearrangements on vesicle structure and

morphology (*Manconi et al. 2012*).
Important structural changes were observed in SAXS patterns of 20glycol-PEVs, especially 5-10DCF 20Trc-PEVs, as a result of a combined effect of both DCFNa and glycols. Indeed, DCFNa promoted bilayer interdigitation, while glycols at high concentration, probably underwent a change of phospholipid partition between vesicle bilayers and water medium. In fact, they decrease the solvent dielectric constant and as a result the number of ionized groups on the interfacial bilayer region (confirmed by lower negative zeta potential). As a final consequence, a partial solubilization of lipid chains of phospholipid on glycol/water medium can be observed, with the formation of interconnected, closely packed or multiwalled vesicles. The SAXS pattern reported in Figure 3D shows the effect of DCFNa and Trc (20%) on 5-10DCF 20Trc-PEVs. Several quasi-Bragg peaks indicating a multilamellar system can be observed in coexistence with other signals. On these basis, according to the cryo-TEM images (Figure 1D), a coexistence of unclosed bilayers and unilamellar vesicles can be supposed.

4.3.5. Rheological studies

To better understand the structural modifications that underwent on vesicle dispersions and to explain the physical state changes from liquid to high viscous liquid or soft-solid like, rheological studies were carried out as well. Frequency sweep and viscometry tests were performed: the storage modulus (G′ at 1 Hz) and viscosity values (at shear rate 1 s−1) were used to compare the viscoelastic properties of the different dispersions. Storage modulus of each formulation was affected by the concentration and in a less extent by the structure of glycols while it was not significantly influenced by the presence of the drug: 5-10DCF liposomes showed a comparable storage modulus value (~1 × 10−2) confirming that these systems were low viscous and unstructured fluids (Figure 4A and B). The storage modulus of PEVs increased as Transcutol

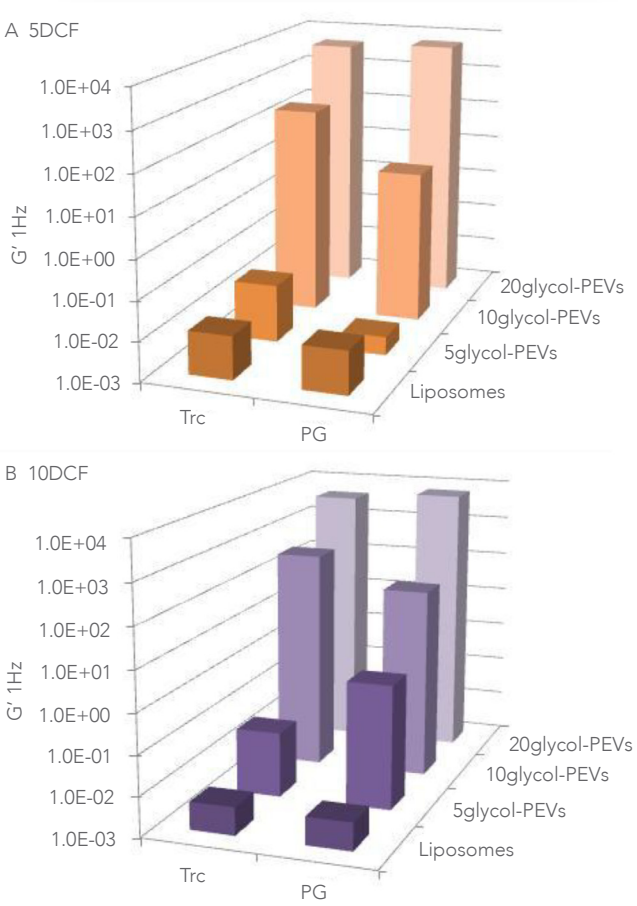

Figure 4. Storage modulus (G') values collected at 1 Hz of 5DCF liposomes and 5DCF glycol-PEVs (A and C) and viscosity data collected at 1 Pa s^{-1} of 10DCF liposomes and 10DCF glycol-PEVs (B and D).

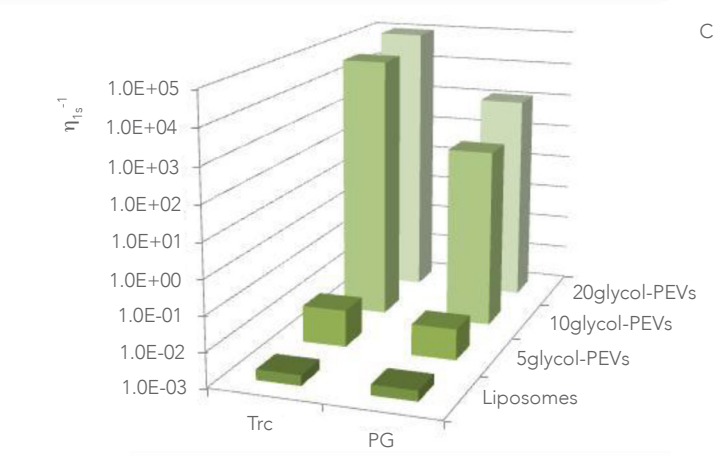
C 5DCF
η_{1s}^{-1}
1.0E+05
1.0E+04
1.0E+03
1.0E+02
1.0E+01
1.0E+00
1.0E-01
1.0E-02
1.0E-03
20glycol-PEVs
10glycol-PEVs
5glycol-PEVs
Liposomes
Trc
PG

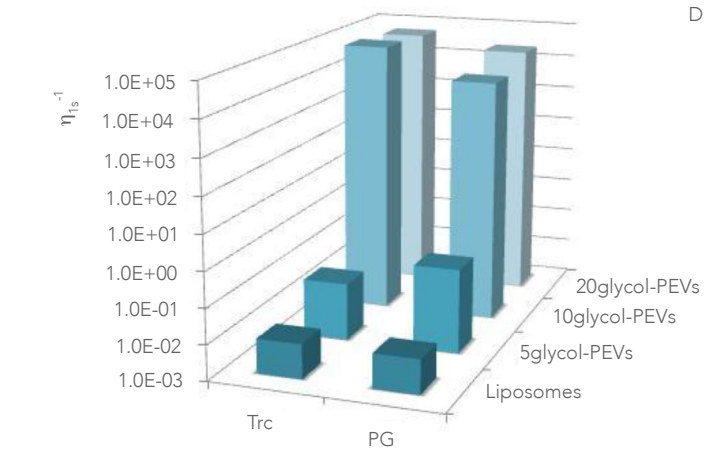
D 10DCF
η_{1s}^{-1}
1.0E+05
1.0E+04
1.0E+03
1.0E+02
1.0E+01
1.0E+00
1.0E-01
1.0E-02
1.0E-03
20glycol-PEVs
10glycol-PEVs
5glycol-PEVs
Liposomes
Trc
PG

or propylene glycol concentration increased reaching values about 3–5 orders of magnitude higher than that of liposomes especially for 5-10DCF 20Trc-PEVs (~4 × 103) and 5-10DCF 20PG-PEVs (~6 × 103) that generated a solid like system probably due to the formation of closely packed and interconnected vesicles. 10glycol-PEVs showed storage modulus values between that of liposomes and that of 5-10DCF 20glycol-PEVs and their macroscopic behavior, as reported in Table 1, was typical of highly viscous liquids or soft-solid (10DCF 10Trc-PEVs). Viscometry experiments (Figure 4C and D) confirmed the above reported observations. As the glycol concentration increased, the viscosity of the system increased correspondingly, 5-10DCF liposomes showed a shear viscosity of about 2 × 10−3 Pa s−1; the presence of glycols at low concentration (5glycol-PEVs) led to a slight increase of system viscosity (~1 × 10−1/−2 Pa s−1) whereas the effect was much more evident in 10-20Trc-PEVs and 10-20PG-PEVs (viscosity ~3 × 105 Pa s−1).

Thermotropic and mechanical properties of vesicle dispersion confirmed that the drug alone was able to modify the internal bilayer packing forming an interdigitated structure but it did not change intervesicle architecture whereas Transcutol and propylene glycol showed a concentration-dependent ability to modify the vesicle assembly as well as the inter-vesicle structure. Glycol presence on water phase led to a reduction of dielectric constant (compared to that of water) and a consequent increase of phospholipid acyl chain solubility in the external medium of vesicles. In this environment phospholipids changed their orientation turning their hydrophobic tails to the glycol/PBS mixture and interacting with other tails of close vesicles to form a tridimensional network of close packed and interconnected vesicles as confirmed by the high values of storage modulus and viscosity. The formation of vesicle interconnections associated to bilayer rearrangements that led to an increase of vesicle size (>155

nm) and lamellarity and to a reduction of free inter-vesicle solvent resulted in macroscopical change of vesicle physical state from liquid to solid for 20glycol-PEVs and 10DCF 10Trc-PEVs.

4.4. Conclusion

This work underlines the significant effects of water miscible cosolvents on phospholipid vesicle assembly structure. Using hydrosoluble glycols such as Trc or PG to prepare hydrogenated soy phosphatidylcholine vesicles entrapping DCFNa, highly viscous liquid or soft-solid system can be obtained thanks to the formation of new interaction forces between drug, glycols and phospholipids. Collected results evidenced the existence of a complex architecture in which vesicles were closely packed and interconnected forming a tridimensional network that is responsible for the high viscous/soft solid like behavior of the system. The highly viscous or solid like systems might facilitate the skin application of drug and increase its residence time at the application site.

5. FABRICATION OF QUERCETIN AND CURCUMIN BIONANOVESICLES FOR THE PREVENTION AND RAPID REGENERATION OF FULL-THICKNESS SKIN DEFECTS ON MICE

Published in Acta Biomaterialia 10, 1292-1300, 2014

5.1. Introduction

Polyphenols are widely distributed in plants and plant-derived foods, including vegetables, fruits, tea, spices, wine, beverages, and nutritional supplement products. In previous studies they have been proposed as therapeutic agents against several acute and chronic diseases, such as Alzheimer and Parkinson, multiplesclerosis, cardiovascular diseases, allergies, and certain types of cancer (*Prasain and Barnes 2007*). These advantages are attributed to their useful antioxidant and anti-inflammatory properties that regulate cell proliferation and function by preventing the onset and progression of the aforementioned diseases (*Lee et al. 1998*) (*Appleton 2003; Nichols and Katiyar 2010; Panchatcharam et al. 2006; Phan et al. 2001*). Although phase I clinical trials have shown polyphenols as safe drugs even at high doses, poor bioavailability, poor absorption, rapid metabolism, and systemic clearance hamper their use in pre-clinical and clinical models. Indeed, polyphenols like curcumin, resveratrol, quercetin, and others, are poorly absorbed in the gastrointestinal tract and undergo fast metabolism by the liver (*Prasain and Barnes 2007; Yallapu, Jaggi, and Chauhan 2012*). Moreover, clinical trials exploring different schedules of administration of polyphenols, especially quercetin (QUE) and curcumin (CUR), have been hampered by their extreme water insolubility (Figure 1). To overcome such limitations, various natural polyphenols have been formulated in innovative nanovesicles to be administered by the dermal route (*Caddeo, Manconi, et al. 2013; Pando et al. 2013*). The topical application of compounds with free-radical scavenging and anti-inflammatory properties in patients has shown a significant improvement in wound healing and protection from oxidative damage. In particular, quercetin and curcumin may be promising for wound healing, thanks to their ability to inhibit reactive oxygen species and tissue inflammation (*Gomathi et al. 2003; Gopinath et al. 2004; Mohanty, Das, and Sahoo 2012; Phan et al. 2001; Süntar et al. 2010*).

Topical chronic non-healing wound is a complex multifactorial process involving the interplay of several cellular and biochemical mechanisms that compromise the viability of superficial tissues (epidermis and dermis). Inflammation, which constitutes a part of the acute response, results in a coordinated influx of neutrophils at the wound site, that produces and releases inflammatory mediators, such as tumor necrosis factor alpha (TNF-α) and interleukin-1 (IL-1). Neutrophils contain high levels of destructive proteases and oxygen free radicals that are released into the local wound area when cells die.

This can cause extensive tissue damage and prolong the inflammatory phase. Non-phagocytic cells also generate free radicals, leading to an accumulation of oxygen and nitrogen reactive species at the wound site. These radicals will result in oxidative stress causing lipid peroxidation, DNA breakage, and enzyme inactivation, including free radical scavenging enzymes (MARTIN n.d.). One of the major causes of delayed healing is the persistence of inflammation or an inadequate angiogenic response (*Appleton 2003*). It has been postulated that an anti-inflammatory response after cutaneous wounding is a prerequisite for healing. Potent antioxidant, anti-inflammatory agents such as quercetin, curcumin and resveratrol, can play an important role in restoring physiological conditions, allowing a significant improvement in wound healing (*Gomathi et al. 2003; Gopinath et al. 2004; Phan et al. 2001*). In the present study phorbol ester 12-O-tetradecanoylphorbol-13-acetate, TPA, has been used to mimic skin inflammation and ulceration caused by oxidative stress. TPA, by activating protein kinase C, stimulates the expression of a wide variety of pro-inflammatory cytokines, such as TNF-α, and causes rapid influx of neutrophils and other innate immune cells into skin. Many of the same physiological effects induced by TPA occur in chronic wound process. Thus, it can be used to mimic chronic skin wound (*Caddeo, Sales, et al. 2013*).

The nanoencapsulation of drugs repre-

Figure 1. Chemical structure of quercetin (A) and curcumin (B).

A

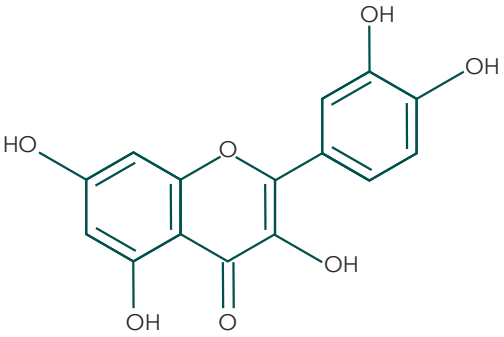

B

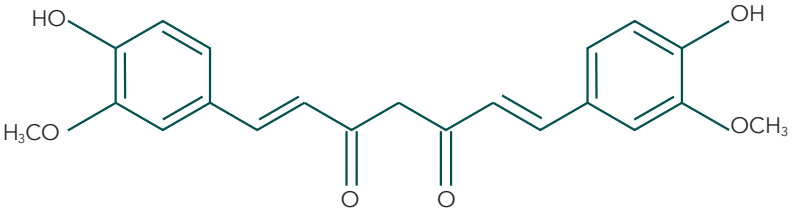

sents the most convenient way of improving their skin delivery. Therefore, during the past two decades many studies have been reported on the use of nanoparticles as carriers for skin delivery. Rationally designed nanocarriers may improve the therapeutic index of drugs, by modifying their pharmacokinetic and biodistribution. The encapsulation of drugs into phospholipid vesicles would significantly alter their in vivo behaviour and many studies have revealed that vesicular drugs should be regarded as new entities different from free (non-entrapped) drugs.
In the present study, quercetin and curcumin were incorporated in liposomes or in innovative Penetration Enhancer containing Vesicles (PEVs) and used as (trans) dermal drug delivery systems. The drug and/or carrier efficacy was evaluated by in vitro skin distribution and in vivo ability to reduce oxidative inflammation and neutrophil infiltration induced by TPA in mice. The inhibition of these factors is a crucial stage to repair chronic wound.

5.2. Materials and methods

5.2.1 Materials

Lipoid S75 (S75), a mixture of soybean phospholipids (70% phosphatidylcholine, 9% phosphatidylethanolamine and 3% lysophosphatidylcholine), triglycerides and fatty acids was purchased from AVG S.r.l. (Milan, Italy). Octyl-decyl polyglucoside (Oramix®CG110, Or) was donated by Seppic (Milan, Italy). Phosphate buffer solution (PBS, pH 7), QUE, CUR, polyethylene glycol 400 (PEG400) and 12-O-Tetradecanoylphorbol 13-acetate (TPA) were purchased from Sigma-Aldrich (Milan, Italy).

5.2.2 Sample preparation

Vesicles were prepared using S75, quercetin or curcumin, PBS for liposomes and PEG400/PBS or Or/PEG400/PBS for PEVs (Table 1). Empty vesicles were used as a reference. All components were weighed in a glass flask, and left hydrating overnight in 5 ml of PBS for liposomes, and PEG400/PBS or Or/PEG400/PBS for PEVs

Table 1. Sample composition and their acronyms.

Sample	QUE or CUR (mg/ml)	S75 (mg/ml)	Oramix (mg/ml)	PEG400 (mg/ml)	PBS (mg/ml)
Control dispersion	-	-	-	50	950
Liposomes	10	240	-	-	1000
PEG-PEVs	10	240	-	50	950
OrPEG-PEVs	10	240	10	50	950

(*Chessa et al. 2011; Manconi et al. 2005*). Then, the suspensions were sonicated (2 seconds on and 2 seconds off, 50 cycles; 13 μm of probe amplitude) with a high intensity ultrasonic disintegrator (Soniprep 150, MSE Crowley, London, United Kingdom). Samples (1 ml) were purified from the non-incorporated drug by dialysis against PBS or appropriate PEG400/PBS or Or/PEG400/PBS mixture (2 L) using dialysis tubing (Spectra/Por® membranes: 12–14 kDa MW cut-off, 3 nm pore size; Spectrum Laboratories Inc., DG Breda, The Netherlands), during 3 hours at 25°C, refreshing the medium twice. QUE and CUR dispersions in PEG400/PBS mixture were used as controls (Table 1).

5.2.3 Vesicle characterization

Vesicle formation and morphology were checked by transmission electron microscopy (TEM) and cryo-TEM. Liposomes were previously diluted (1:2) with PBS and PEVs with PEG400/PBS or Or/PEG400/PBS. TEM observation was carried out using a JEM-1010 (Jeol Europe, Croissy-sur-Seine, France) microscope, equipped with a digital camera, at an accelerating voltage of 80 kV. A drop of diluted vesicular dispersion was applied to a carbon film-covered copper grid for 5 minutes, subsequently dispersion was absorbed with filter paper and stained with a 1% phosphotungstic acid.

For cryo-TEM analysis, a thin aqueous

film was formed by placing a drop of diluted sample (1:2) on a glow-discharged holey carbon grid and then blotting the grid against filter paper. The resulting thin films spanning the grid holes were vitrified by plunging the grid into ethane, which was maintained at its melting point with liquid nitrogen, using a Vitrobot (FEI Company, Eindhoven, The Netherlands). The vitreous films were transferred to a Tecnai F20 TEM (FEI Company) using a Gatan cryotransfer (Gatan, Pleasanton, CA), and the samples were observed in a low dose mode. Images were acquired at 200 kV at a temperature between –170/-175°C, using a CCD Eagle camera (FEI Company, Eindhoven, The Netherlands).

The average diameter and polydispersity index (PI, as a measure of the size distribution width), were determined by Photon Correlation Spectroscopy (PCS) using a Zetasizer nano-ZS (Malvern Instruments, Worcestershire, United Kingdom). Samples were backscattered by a helium-neon laser (633 nm) at an angle of 173° and a constant temperature of 25°C. Just before the analysis, samples were diluted 1:1000 using PBS for liposomes and PEG400/PBS or Or/PEG400/PBS for PEVs to avoid alteration of intervesicle environment.

Zeta potential was estimated using the Zetasizer nano-ZS by means of the M3-PALS (Mixed Mode Measurement-Phase Analysis Light Scattering) technique, which measures the particle electrophoretic mobility.

Entrapment efficiency (EE%), expressed as the percentage of the amount of drug initially used, was determined by high performance liquid chromatography (HPLC) after disruption of vesicles with 0.025% non-ionic Triton X-100. QUE and CUR content was quantified at 367 and 424 nm respectively, using a chromatograph Alliance 2690 (Waters, Milano, Italy). The column was a SunFire C18 (3.5 µm, 4.6×150 mm). The mobile phase was a mixture of acetonitrile, water and acetic acid (94.8:5:0.2, v/v), delivered at a flow rate of 1.0 ml/min.

The lipid content of dispersions was

determined by the Stewart assay (45). Briefly, an aliquot of suspension was added to a biphasic mixture of aqueous ammonium ferrithiocyanate solution (0.1 N) and chloroform. The concentration of S75 was obtained by measuring absorbance at 485 nm in the organic solution. The aggregation efficiency (AE%) represented the effective amount of aggregated phospholipids expressed as the percentage of the amount initially used.

5.2.4 Small- and Wide-Angle X-ray Sacattering (SWAXS)

SWAXS experiments were carried out using a S3-MICRO (Hecus X-ray systems, Graz, Austria) coupled to a GENIX-Fox 3D X-ray source (Xenocs, Grenoble, France) and a 50 focused X-ray beam with 0.1542 nm at Cu Kα-line. The q range was 0.003-0.6 Å−1 for SAXS and 1.3-1.9 Å−1 for WAXS, where $q = (4 \pi \sin \theta)/\lambda$ is the modulus of the scattering wave vector, θ the scattering angle and λ the wavelength. The analysis of the dispersions was carried out at their native concentration. All scattering curves, recorded at 25°C were reproduced twice, and a representative curve was selected, plotting the scattering intensity (I) as a function of the scattering vector (q). SAXS patterns were analyzed in terms of a global model using the program GAP (Global Analysis Program) developed by Pabst (46) that permitted to obtain relevant structural parameters on bilayer-based structures, i.e. vesicles and lamellar phases. From the analysis, the membrane thickness was obtained through the definition $dB = 2 (zH + 2 \sigma H)$. zH and σH derive from SAXS curve fitting with GAP.

5.2.5 In vitro skin penetration and permeation studies

Experiments were performed on new born pig skin using Franz vertical cells with an effective diffusion area of 0.785 cm2, under non-occlusive conditions. The skin, stored at –80°C, was pre-equilibrated in saline (0.9% w/v of NaCl) at 25°C. Skin specimens (n = 6 per formulation) were

sandwiched between donor and receptor compartments. The receptor was filled with 5.5 ml of saline, continuously stirred and thermostated at 37± 1˚C. Samples (20 µl) were applied onto the skin surface at 0 and 3 h. At regular intervals, up to 24 h, the receiving solution was withdrawn, replaced with pre-thermostated (37˚C) fresh saline and analyzed by HPLC for drug content. After 24 h, the skin surface was gently washed (3 times) with 1 ml of distilled water, then dried with filter paper. The stratum corneum was removed by stripping with adhesive tape Tesa® AG (Hamburg, Germany). Epidermis was separated from dermis with a surgical scalpel. Tape strips, epidermis, and dermis were cut, placed each in a flask with methanol and sonicated for 4 minutes in an ice bath to extract the drug. The tapes and tissue suspensions were filtered out and assayed for drug content by HPLC.

5.2.6 In vivo oedema and myeloperoxidase assays

Female Hsd:ICR(CD-1®) mice (5-6 weeks old, 25-35 g) were obtained from Harlan Laboratories (Barcelona, Spain) and acclimatized for 1 week before use. All studies were performed in accordance with European Union regulations for the handling and use of laboratory animals. The protocols were approved by the Institutional Animal Care and Use Committee of the University of Valencia.

The back skin of mice was shaved and TPA dissolved in acetone (243 µM; 3 µg/20 µL) was applied to the shaved dorsal area (~ 2 cm2) to induce cutaneous inflammation and ulceration (day 1) (figure 2). Negative control mice received acetone only (20 µL). All test compounds (20 µL), were topically smeared over the same dorsal site 3 and 6 h after TPA application. The procedure was repeated (at 24-h intervals) on day 2 and 3. On day 4, mice were sacrificed by cervical dislocation. Each group comprised four mice (figure 3). The inhibitory effect of test compounds on inflammation and ulceration was determined by two biomarkers: oedema formation and myeloperoxidase

Figure 2: In vivo inflammatory studies

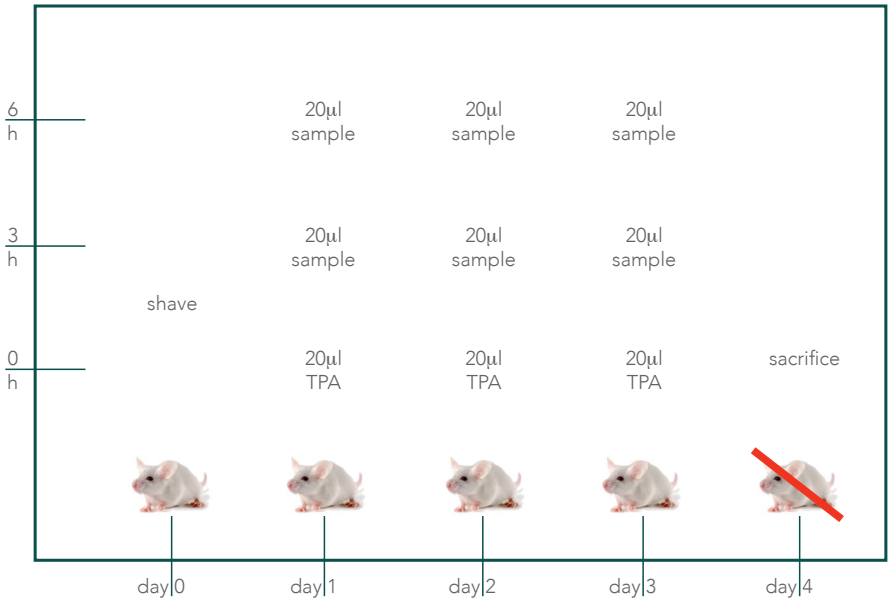

Figure 3: Schematic representation of the study

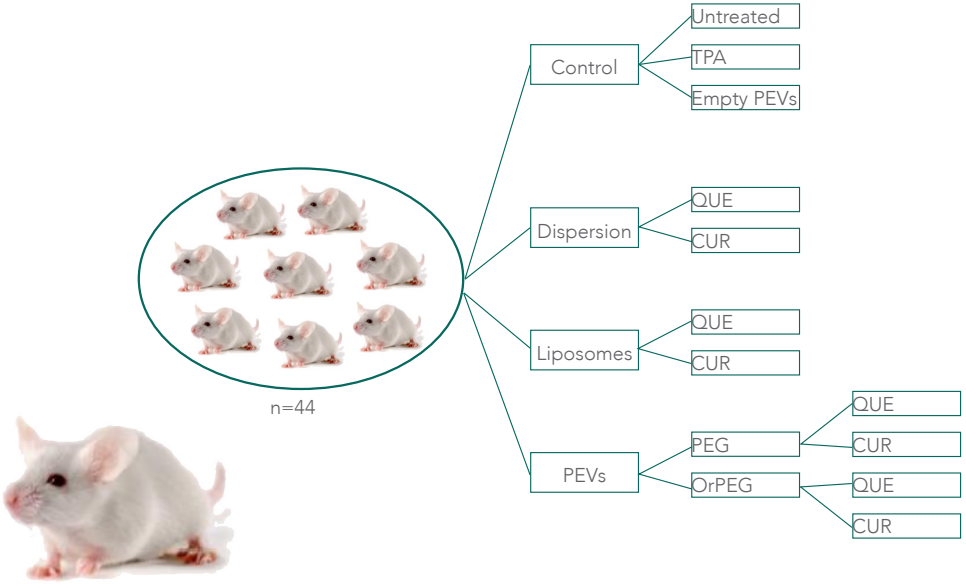

(MPO) activity. The dorsal treated skin area of sacrificed mice was excised, weighed to assess any increase indicative of oedema formation. MPO assay was performed following the previously reported method (Caddeo, Sales, et al. 2013; Sato et al. 1996). Briefly, skin biopsies were homogenized and centrifuged, the supernatant was incubated with hydrogen peroxide and tetramethylbenzidine and then assayed for MPO activity spectrophotometrycally at 620 nm. The MPO activity was calculated from the linear portion of a standard curve.

5.2.7 Histological examination

Skin biopsies (~ 2 cm2) were excised from mice treated region, after 72 hours of treatment (on day 4), and maintained in formaldehyde (10% v/v). Tissue samples were processed routinely and embedded in paraffin wax. Longitudinal sections (5 μm) were stained with haematoxylin and eosin. Microscopic assessment by light microscope was performed blind on coded slices.

5.2.8 Statistical analysis of data

Results are expressed as the mean±standard deviation. Analysis of variance (ANOVA) and Bartlet's test for homogeneity of variance were performed using IBM SPSS statistics for Windows. Post hoc testing ($P < 0.05$) of the multiple comparisons was performed by the Scheffe or Dunnet tests.

5.3. Results

The chemical structure of polyphenolic QUE and CUR is reported in Figure 1. QUE is a yellow-green, polyphenolic flavonol containing the 3-hydroxyflavone backbone with 5 oxydrilic groups in position 3'-4' and 3-5-7 (Figure 1A). CUR is a yellow-orange polyphenol formed by two aromatic o-methoxy phenolic groups, linked by a seven-carbon chain with a β-diketone (Figure 1B). Under physiological conditions, CUR can exist in both an enol and a bis-keto form, which coexist in equilibrium. These phytochemicals were entrapped in phospholipid vesicles and

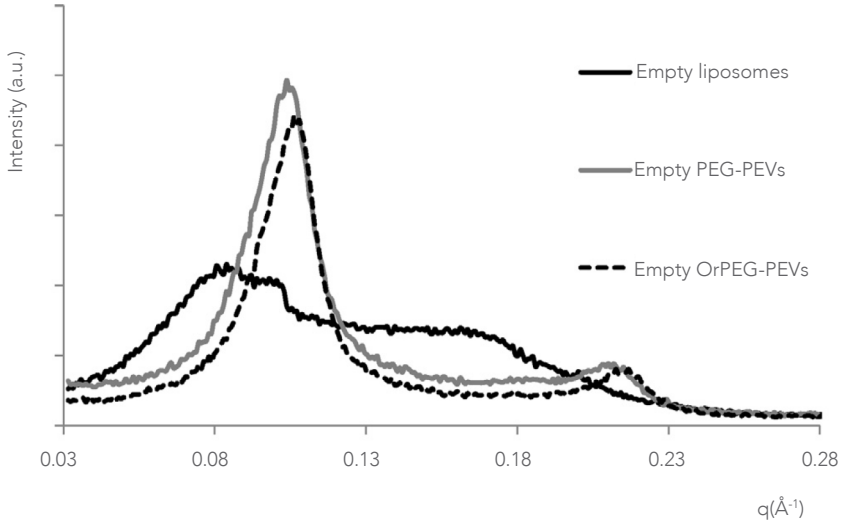

Figure 3. Representative SAXS diffraction profiles of empty liposomes and PEVs.

the results of their nanoformulation and application on the skin are presented. All the vesicles were prepared using S75, a mixture of soybean lipids containing mainly phosphatidylcholine, and in minor amounts phosphatidylethanolamine, lysophosphatidylcholine, triglycerides and fatty acids (Table 1). S75 was used at a high concentration (240 mg/ml) to efficiently entrap 10 mg/ml of phytodrugs. To prepare PEVs, one (PEG400) or two (PEG400 and Oramix) hydrophilic surfactants were added to the water phase. Table 2 summarizes the physicochemical features of the prepared liposomes and PEVs.

Empty liposomes' size was 121±8 nm, and the addition of the surfactants resulted in an increase in size ($p<0.05$) that was more evident when surfactants were simultaneously used in OrPEG-PEVs ($p<0.01$). The presence of quercetin did not affect vesicle size ($p>0.05$), while curcumin caused an enlargement of vesicles. Particle

Table 3. Selected fitting parameters and derived parameters for SAXS curves (n=3) of empty and QUE or CUR loaded vesicles. Vesicles were oligolamellar (OLV) or multilamellar (MLV). All distances are given in Å: repetition distance or lamellar thickness (d); polar head amplitude (σ_h); polar head distance to the centre of bilayer corresponding to lipid half extent (Z_h); bilayer thickness (d_B), water layer thickness (d_W).

Sample	structure	Z_h	σ_h	d	d_B	d_W
Empty liposomes	OLV	17±05	3±0.4	78±0.4	46±2	32±1
Empty PEG-PEVs	MLV	17±03	4±0.4	61±0.1	52±2	8±1
Empty OrPEG-PEVs	MLV	16±03	6±0.3	60±0.1	55±2	5±1
QUE liposome	OLV	17±0.5	3±0.3	74±0.5	47±3	27±2
QUE PEG-PEVs	MLV	16±0.6	5±0.5	60±0.2	53±2	7±1
QUE OrPEG-PEVs	MLV	16±0.4	6±0.3	60±0.3	54±2	6±1
CUR liposomes	OLV	17±0.7	4±0.4	72±0.3	49±2	23±2
CUR PEG-PEVs	MLV	16±0.3	6±0.2	60±0.2	55±3	5±1
CUR OrPEG-PEVs	MLV	16±0.4	6±0.6	59±0.3	54±3	5±1

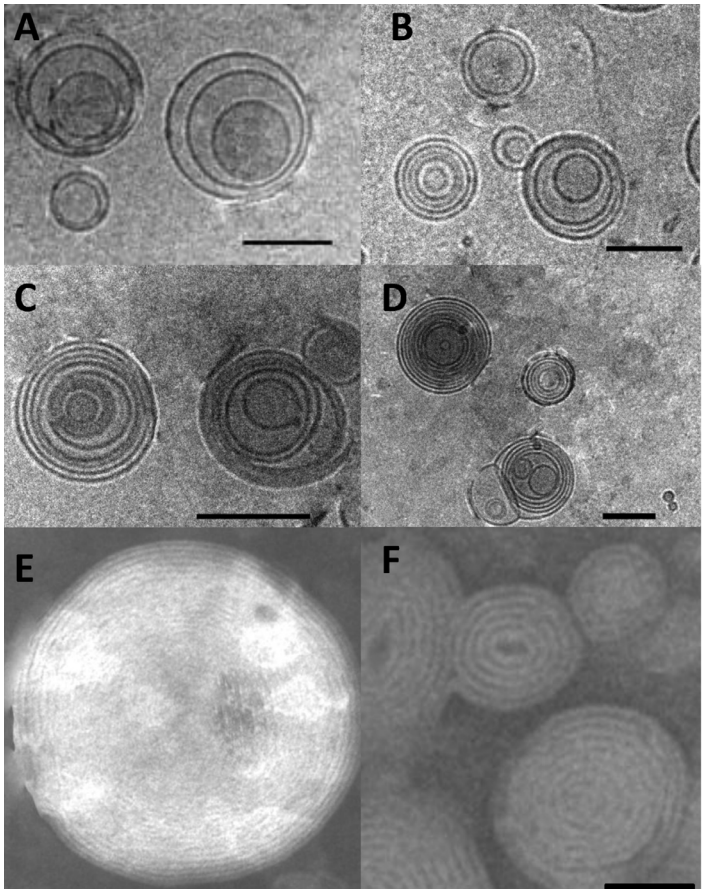

Figure 2. Cryo-TEM micrographs of QUE-loaded liposomes (A), CUR-loaded liposomes (B), QUE-loaded PEG-PEVs (C) and CUR-loaded PEG-PEVs (D). Negative stain TEM micrographs of QUE-loaded OrPEG-PEVs (E) and CUR-loaded OrPEG-PEVs (F). Bars represent 100 nm.

size distribution was broad (PI<0.37) but always repeatable and was smaller for quercetin-loaded vesicles (PI<0.26). Zeta potential value was slightly negative (~ -10 mV) for all the samples, independently of their composition. Incorporation efficiency was ~ 64% for both drugs, without statistical differences (p>0.05) among liposomes and PEVs. Aggregated phospholipids were around 70% in liposomes and around 63% in PEVs, probably due to their partial solubilisation by PEG400.

Vesicle formation and morphology were confirmed by TEM and cryo-TEM investigation (Figure 2). Vesicles appeared always spherical and lamellar, but the number of lamellae increased in the presence of PEG400 (PEVs).

Complementary information on vesicle structure can be obtained from SWAXS studies that permit to explore the molecular packing of phospholipids in both head group and acyl chain regions. The WAXS patterns of all tested vesicles were characterized by a very diffuse scattering, without evident signal, confirming the vesicle state in liquid-crystalline form in which the lipid acyl chains of bilayer are disordered (data not shown). Representative SAXS diffractograms and deduced parameters are reported in Figure 3 and Table 3.

Analyzing the curves of empty and loaded liposomes, only a first order sharp diffraction peak is observed at 0.08 Å-1 with a shoulder at 0.09 Å-1, which indicates the presence of a small population of oligolamellar vesicles (2-5 bilayers). The presence of PEG400 and Oramix in PEVs altered the patterns: a sharp reflection is observed at 0.10 Å-1 with a symmetric profile, and a second order peak at 0.21 Å-1, confirming the change to multilamellar structures (Figure 3). The patterns of QUE and CUR liposomes and PEVs were similar to that of empty vesicles.

In comparison with empty liposomes, PEVs showed a higher polar head amplitude (σH, from 3 to 6 Å) and bilayer thickness (dB, from 46 to 55 Å), while their polar head distance to the centre of the bilayer, corresponding to lipid half extent

(zH, from 17 to 16 Å), and the repetition distance or lamellar thickness (d, from 78 to 60 Å) were lower. The most significant modification of SAXS parameters was observed in the reduction of water layer thickness (dw) that in liposomes was ~ 27 Å and in PEVs decreased to ~6 Å, showing a significant contraction of interlamellar spaces in the presence of hydrophilic surfactants. The trend was the same for QUE and CUR liposomes and PEVs. Concerning the interaction of phytodrugs with liposomal bilayer, QUE led only to a slight reduction of lamellar thickness (d, from 78 to 74 Å), whereas CUR increased both the polar head amplitude (σH, from 3 to 4 Å) and the bilayer thickness (dB, from 46 to 49 Å) and reduced the lamellar thickness (d, from 78 to 72 Å).

Skin delivery capability of QUE- and CUR-loaded liposomes and PEVs was evaluated in vitro under non-occlusive conditions using Franz diffusion cells (Figure 4). Quercetin and curcumin deposition and permeation were similar: the highest accumulation was reached in the stratum corneum, with a minimum value (15%) for drug dispersions and a maximum value (~28%) for liposomes and PEVs ($p>0.05$). Drug deposition in epidermis was lower for all the formulations and control dispersions, and ranged from 1.5% for drug dispersions and curcumin-loaded OrPEG-PEVs to 3.1% for the other ones. The accumulation in dermis and receptor fluid was even lower (≤1%) and without statistical differences among the different formulations ($p>0.05$).

As previously reported, TPA daily applied on dorsal mouse skin during 3 days induced skin ulceration (~2 cm^2), loss of epidermis integrity, crust formation and biological alterations on dermis and subcutaneous tissue (Caddeo, Sales, et al. 2013). Histopathological analysis of hematoxylin and eosin stained TPA-treated skin revealed the complete absence of epidermis in the central area of injury and a marked infiltration of leukocytes (neutrophils and eosinophils) in dermis, subcutaneous and muscle tissue, and a severe vascular congestion (Figures 5C

and D). Skin treated with TPA and subsequent quercetin or curcumin dispersions, showed an extensive damage of epithelium with localized keratinization in several sites, an evident infiltration of leukocytes in dermis and in subcutaneous tissue and vascular congestion (Figure 5E).

In TPA-inflamed skin subsequently treated with QUE and CUR bionanovesicles, there were areas extensively keratinized with thick crusts and others with a thin layer of migrating epithelium over the dermis, indicating the epidermis reformation. Leukocyte infiltration was less severe, especially in dermis, and congestion of blood vessels was less evident (Figures 5F and G). In CUR PEG-PEVs an extensive reepithelization of the skin with multiple layers of thick epidermis was observed. Connective tissue, and collagen fibres were arranged, leukocyte infiltration was moderate and limited to ipodermis and no vessel congestion was observed (Figure 5H).

When TPA treatment was associated (after 3 and 6 h) to quercetin or curcumin local applications, the skin lesion and inflammation were inhibited, depending on the polyphenol and the carrier used. All the tested samples, even empty vesicles and quercetin and curcumin dispersions suppressed TPA-induced oedema ($p<0.05$) and showed an oedema inhibition ranging from 50 to 91%. Curcumin-loaded PEG-PEVs provided the highest oedema inhibition (91%): this value was statistically different from the other curcumin formulations (Table 4). The level of MPO activity is directly proportional to the neutrophil concentration in the inflamed tissue. In this work, we used MPO activity as a quantitative assay to evaluate the polyphenol anti-inflammatory efficiency in wound tissue (Table 4). Quercetin- and curcumin-loaded liposomes and PEVs showed a superior ability, over phytodrug dispersions, to reduce MPO activity in damaged tissue and the inhibition value was higher, especially for quercetin liposomes (59%) and curcumin liposomes and PEG-PEVs (~68%). Quercetin PEVs

achieved only 40% of MPO inhibition and the other samples did not have statistical significance, as compared to the TPA-treated skin.

5.4. Discussion

In the present investigation effective phospholipid bionanovesicular formulations were developed to achieve maximum loading capacity and optimal skin delivery of two natural phytodrugs: quercetin and curcumin. Despite their different structure, quercetin and curcumin are two polyphenolic phytochemicals with comparable pharmacological antioxidant and anti-inflammatory activities (*Davis, Murphy, and Carmichael n.d.; Liu 2003; Panchatcharam et al. 2006; Phan et al. 2001*). Both these polyphenols have been proposed as topical therapeutic agents for skin irritation and skin barrier function recovery in wound healing, because they

Sample	MD (nm±SD)	PI	ZP (mV±SD)	EE (%±SD)	AE (%±SD)
Empty liposomes	121±8	0.26	-11±2	-	-
Empty PEG-PEVs	138±10	0.30	-11±3	-	-
Empty OrPEG-PEVs	160±11	0.31	-10±4	-	-
QUE liposome	112±9	0.25	-10±4	68±7	79±4
QUE PEG-PEVs	132±8	0.26	-10±3	58±8	62±6
QUE OrPEG-PEVs	152±11	0.23	-11±2	56±6	58±8
CUR liposomes	161±12	0.33	-13±2	71±8	82±9
CUR PEG-PEVs	188±9	0.34	-11±3	68±7	66±8
CUR OrPEG-PEVs	220±13	0.37	-9±4	64±9	65±7

Table 2. Mean diameter (MD), polydispersity index (PI), zeta potential (ZP), entrapment efficiency (EE) and aggregation efficiency (AE) of empty and quercetin (QUE) or curcumin (CUR) loaded vesicles. Mean values±standard deviation (SD) were obtained from at least 6 samples.

can modulate inflammation and angiopathy, the major issues associated with impaired wound healing (*Gomathi et al. 2003; MARTIN n.d.; Mohanty et al. 2012; Panchatcharam et al. 2006; Sidhu et al. n.d.*). The cutaneous application of nanoencapsulated drugs may improve therapeutic effectiveness by extended time of local action at higher concentrations, and may reduce the risk for systemic side effects.

To optimize the maximum amount of drug that could be loaded in phospholipid vesicles, a pre-formulation study was carried out using several phospholipids and different amounts of drug and phospholipids (data not reported). Among the tested phospholipids, S75 was found to produce the vesicles loading the highest amount of both quercetin and curcumin, which was 10 mg/ml. Such concentration allowed the bilayer and water phase of vesicle dispersion to be saturated and such condition can facilitate drug passage across the skin. Indeed, the maximum drug transfer into the skin takes place when the vehicle is saturated with the drug, because it is in a state of elevated thermodynamic activity that confers a greater leaving tendency (51, 73). Saturated conditions are therefore preferable for topical drug delivery systems. Conventional liposomes and innovative phospholipid vesicles (PEVs) were prepared using a high amount of S75 and the same amount of quercetin and curcumin. These polyphenols are lipophilic molecules that can localize in the bilayer of vesicles, and to stabilize 10 mg/ml of the phytodrugs into the lamellar structure, a high concentration of lipids (240 mg/ml) is needed. Otherwise, drug precipitation occurs, especially using curcumin.

Moreover, in PEVs, PEG400 and Oramix were added to improve drug solubility and diffusion through the skin (Table 1) (5, 9, 67, 74). They are nonionic surfactants (Oramix, HLB =16; PEG400 HLB 20) able to increase skin permeation of drugs by causing a disordering effect within its intercorneocyte lamellar phase (75). PEVs were prepared with and without Oramix

to evaluate its possible synergistic effect with PEG400 allowing an additional benefit on drug activity.

In this study, thanks to the use of different and sophisticated techniques such as TEM, light scattering, electrophoretic measurements and x-ray scattering, we gained a precise and detailed picture of quercetin and curcumin nanovesicle structure, which represents an important ground to evaluate their effectiveness in vitro and in vivo.

Liposomes were oligolamellar vesicles with spherical shape and homogeneous size distribution, whereas PEVs were always multilamellar and larger than liposomes. Due to their different chemical structure, quercetin and curcumin differently affected vesicle features. The characterization of formulations showed that the incorporation of tricyclic quercetin did not affect vesicle size, probably because its chemical structure and spatial arrangement was not able to modify bilayer packing. On the contrary, bicyclic curcumin caused an enlargement of the vesicle curvature radius, an increase in lamellarity and, consequently, in size. In particular, curcumin, in liposomes, seems to have a more pronounced disturbing effect on the polar head amplitude, probably due to its more superficial localization in the bilayer (76). The presence of curcumin enlarged the polar head area and consequently bilayer thickness and curvature. Such effects were more evident when hydrophilic surfactants were used (PEVs). Their presence, in synergy with polyphenols, modified the lamellar packing, increasing the vesicle size, lamellarity, polar head amplitude and, slightly, lipid bilayer amplitude, as compared to the corresponding liposomes. These physical rearrangements were combined with a reduction of lamellar and water layer thickness due to a partial shielding effect of these molecules on bilayer surface that reduced interbilayer repulsion and their consequent distance.

Given all that, empty and quercetin-loaded liposomes were the smallest vesicles with the lowest polar head amplitude,

and curcumin OrPEG-PEVs were the largest ones with the highest polar head amplitude, as well as the other OrPEG-PEVs. Zeta potential values were similar for all the tested formulations due to the presence of phosphatidylcholine, the main component of the bilayer, which is a zwitterionic molecule containing the phosphate and choline functional groups: at pH near neutrality (~7) it shows the prevalence of charged phosphate group imparting a negative value to the vesicle surface (50, 77).

In vitro skin permeation study represents a valid and alternative method to select effective formulations able to exert optimal properties in vivo. Given the limited availability of human tissue and the fact that a number of percutaneous investigations may be too toxic to be carried out on living subjects, in vitro animal models have been investigated for their usefulness in predicting cutaneous and percutaneous absorption mechanisms and kinetics. Several studies suggest that pig skin can be used as an excellent surrogate for human skin in vitro dermal and transdermal tests (78, 79). In particular, new born pig skin is a reliable, feasible model, superior to other animal species, for the evaluation of drug penetration and permeation, thanks to the similarity of its stratum corneum in terms of lipid composition, even if it presents a marked difference in terms of thickness. New born pig stratum corneum is considerably thinner than that of adult pigs, and more similar to that of the human skin, even if the number of hair follicles is higher (6, 80). In the light of this, in the present work the skin permeation ability of QUE and CUR nanovesicles was evaluated in vitro using new born pig skin.

Saturated dispersions of QUE and CUR (containing 50 mg/ml of PEG and 950 mg/ml of PBS) were used as controls to obtain free drug deposition into the skin in the absence of a nanocarrier, exploiting only the penetration enhancer ability of PEG400. It can improve drug solubilisation and facilitate its passage through the stratum corneum barrier by temporarily

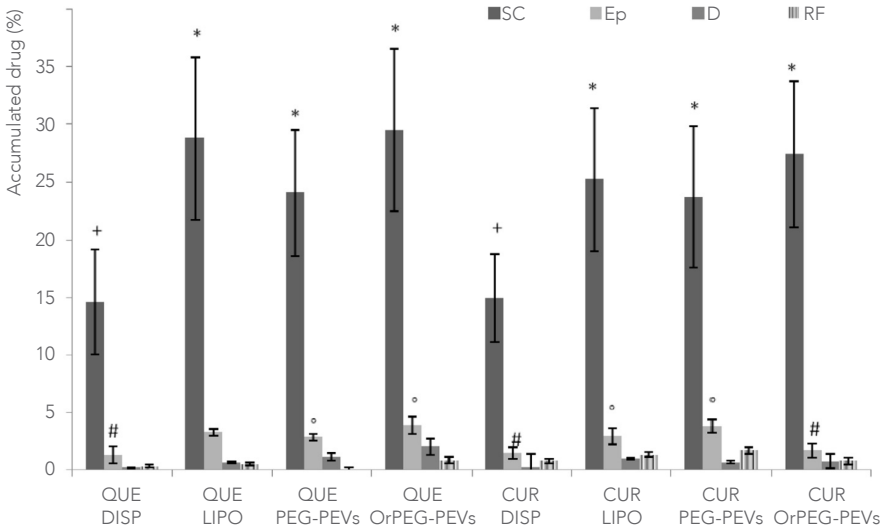

Figure 4. Determination of QUE and CUR deposition into skin layers (SC, stratum corneum; Ep, epidermis; D, dermis) and receptor fluid (RF) after 24 h of non-occlusive treatment with drug dispersions, liposomes and PEVs. Each value is the mean±SD of at least six experimental determinations. No statistical differences ($p>0.05$) were found between samples labelled with the same symbol (*, +, #, °).

perturbing interlamellar structure. Using control dispersions, drug deposition into the skin was 15% in the stratum corneum, 1.5% in epidermis and 0.2% in the dermis. Skin permeation involves diffusion across a series of barriers and anatomical structures that make difficult drug passage. Lamellar vesicles, like liposomes and PEVs, can facilitate drug diffusion into or through the skin, depending on their ability to act as penetration enhancers or drug carriers. Actually, both liposomes and PEVs were able to improve QUE and CUR skin deposition, with respect to drug dispersions, especially in the stratum corneum where they reached ~28%, ~3% in epidermis (except for curcumin Or-PEG-PEVs) and ~1% in the dermis. These findings show that using liposomes and PEVs an additional benefit on drug accumulation in the skin can be achieved, as they act not only as penetration enhancers, but also as suitable carriers.

Skin irritation and local inflammation in the TPA model occurred within 1-4 h due to increased vascular permeability and the following development of oedema and swelling in the dermis. As a result, polymorphonuclear leukocytes migrate to the dermis within about 24-48 h and may be estimated by the MPO assay. Indeed, TPA induces inflammation, leukocyte infiltration, accumulation of oxygen free radicals and subsequent epidermal damage mimicking some of the effects of chronic skin wounds. The ability of QUE and CUR nanovesicles to inhibit oedema and MPO during TPA treatment allowed stopping the biochemical events that naturally lead to wound formation. The topical administration of polyphenol-loaded nanovesicles achieved an important reduction of epidermal loss, local vascular permeability and leukocyte infiltration.

QUE and CUR dispersions were unable to achieve the same biochemical effects on TPA-treated tissue: skin appeared inflamed and damaged, and MPO inhibition was not significant ($p>0.05$). We can state that bionanovesicles play a key function in actively carrying the phytodrugs to the

dermis where they facilitate drug uptake by fibroblasts. CUR and QUE promotion of wound healing has been previously studied, but their intrinsic activity and potential efficacy in carriers were not compared before (62, 63). Quercetin-loaded vesicles were more effective than empty vesicles in inhibiting MPO accumulation and leukocyte infiltration in damaged tissue, but their ability to reduce oedema formation was similar to empty phospholipid vesicles that also possessed a good antioedema activity.

Curcumin vesicles, especiallyCUR PEG-PEVs, showed the best ability to reduce oedema and MPO activity (91% and 67%, respectively), not just for its intrinsic higher pharmacological activity (marginal for curcumin dispersion), but probably because this formulation possesses a su-

Sample	Oedema (mg)	Oedema I (%)	MPO (ng/mg)	MPO I (%)
Untreated	4.1±0.13	100	0	100
TPA	10.2±0.76	0	275±17	0
Empty OrPEG-PEVs	*5.3±0.63	80±6	277±7	0
QUE dispersion	*5.0±0.51	85±5	277±8	17±3
QUE liposomes	*4.9±0.82	86±8	°113±11	59±4
QUE PEG-PEVs	*5.3±0.55	74±5	+°167±9	39±3
QUE OrPEG-PEVs	*5.5±0.69	76±7	+°140±17	49±7
CUR dispersion	+*7.1±0.36	50±4	244±19	11±7
CUR liposomes	+*6.5±0.29	61±3	#°86±11	69±4
CUR PEG-PEVs	#°4.6±0.62	91±6	#°90±18	67±7
CUR OrPEG-PEVs	*5.9±0.96	70±9	+*201±6	27±3

Table 4. Mouse oedema and myeloperoxidase (MPO) values (n=4) and relative oedema and myeloperoxidase inhibition (I%), obtained after TPA treatment followed by application of QUE and CUR dispersions, liposomes and PEVs. Symbols * ($p<0.05$), ° ($p<0.01$) indicate statistical differences with respect to TPA-treated mouse; symbol # indicates statistical difference with respect to +.

perior ability to load curcumin and carry it across the skin in the damaged tissue, potentiating its therapeutic efficacy (72). The inhibition of skin damage by curcumin nanovesicles may be due to the inhibition of detrimental activity of reactive oxygen species (ROS) that leads to a protective effect on fibroblasts, increasing their proliferation and their production of collagen and elastin (81). These fibrous proteins play a central role in wound healing, being main components of connective tissue that provides a structured and organized connective network for the regenerating tissue (82, 83). The specific mechanism by which polyphenols prevent skin ulceration and enhance early regeneration of wounds is not exactly explained. However, it is commonly recognized that several concomitant factors may be involved. Some research reported the beneficial effect of polyphenols on early repair of ulcers due to improvements on cell regeneration and collagen synthesis that can be in part related to their antioxidant and free-radical scavenging activity able to reduce cell damage and apoptosis (58, 66, 82, 83). For the same reason, they may also provide a protection of hematopoietic system, facilitating the reduction of the tissue homeostasis (83). Further, it has been reported that they are able to increase the synthesis of anti-inflammatory prostaglandins responsible for the accelerated healing.

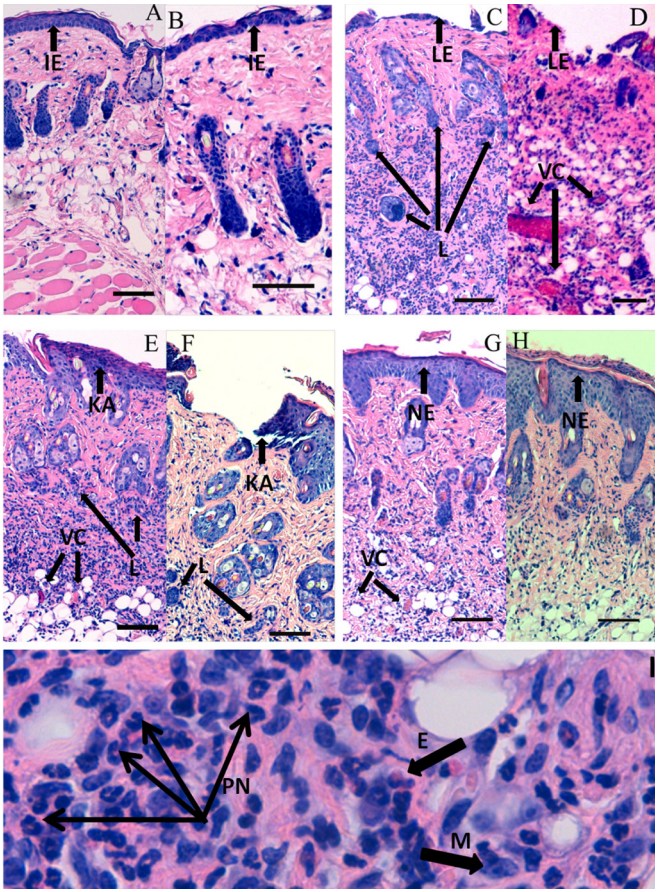

Figure 5. Histopathological examination of hematoxylin-eosin stained mouse skin section: untreated (A and B), TPA-inflamed (C and D) or TPA-inflamed and treated with quercetin dispersion (E), quercetin liposomes (F), curcumin OrPEG-PEVs (G) and curcumin PEG- PEVs (H). Bars represent 100 ?m. Intact epidermis (IE), loss of epidermis (LE), leukocyte (L), vascular congestion (VC), keratinized areas (KA) and new epidermis (NE) are arrowed. A magnification (60x, I) of the inflamed skin is shown with arrowed polymorphonuclear neutrophils (PN), eosinophils (E), macrophages (M).

5.5. Conclusion

Results on quercetin and curcumin bionanovesicles show their significant anti-inflammatory activity able to inhibit the onset of skin wound during the TPA treatment. This protective effect was more relevant in curcumin PEG-PEV formulation thanks to the excellent ability of the vesicle carrier to increase drug bioavailability in the target tissue. Nanoentrapped curcumin prevented the formation of skin lesions abrogating the various biochemical processes that cause epithelial loss and skin damage. Based on the epidemiological evidence and in vivo and in vitro studies we can suggest that a daily topical application of curcumin-loaded nanovesicles on patients at higher risk of skin wound may provide efficient protection against this compliance.

6. GENERAL CONCLUSION

In this study skin specific delivery systems were prepared, characterized and subjected to in vitro, ex vivo and in vivo studies.

We used a different amount of penetration enhancer to improve drug incorporation into the phospholipid bilayered vesicles and drug delivery to the skin. Indeed, results have underlined the ability of the studied PEVs to reach these aims. Thanks to the presence of the penetration enhancers, quercetin and curcumin were incorporated in high yields into the new PEVs. Moreover, the association of penetration enhancer to the liposomal vesicles has increased drug deposition into the skin, thus showing that PEVs are potent nanocarriers for skin delivery.

This research has produced three papers: in the first work it has been shown that concentrated and densely packed transcutol containing vesicles are valuable candidates for topical drug delivery of the NSAID diclofenac. These new carriers are able to form a gel-like interconnected vesicular dispersion that is characterized of a viscosity higher than that of water, favoring the cutaneous drug deposition and interaction with fibroblasts. In vitro studies with cells have proved that these PEVs are capable of being internalized by the 3T3 fibroblasts and, also, of reducing the in vitro drug toxicity.

The second paper has highlighted the important effects of water miscible co-solvents, such as propylene glycol, on hydrogenated phospholipid vesicle assembly structure. Results showed the presence of a complex architecture in which vesicles are closely packed and interconnected forming a tridimensional structure that is responsible for the high viscous/soft solid like behavior of the system. This complex structure facilitates the topical application of the formulation (without the need of using jellifying polymers that would affect the drug release) and increase the drug residence time at the application site.

Results of the third paper has shown evidence of an important anti-inflammatory activity of the quercetin- and curcu-

min-loaded bionanovesicles capable of inhibiting the onset of skin wound during the TPA treatment. The most protective effect was relevant in curcumin PEG-PEV formulation thanks to the capability of the vesicle carrier to increase drug bioavailability in the target tissue. Indeed, ex vivo penetration and permeation results have shown that the presence of a hydrophilic penetration enhancer molecule in the formulation is crucial for improving dermal delivery of a lipophilic drug such as curcumin or quercetin.

Summarizing the results of this study, PEVs can be a promising formulation for (trans)dermal delivery of both hydrophilic and lipophilic drugs.

In conclusion, PEVs are eligible for the use as suitable carriers in skin disease treatment.

6. General conclusion

7. REFERENCES

1. A. Jadoul, J. Bouwstra, V. Praat. *Effects of iontophoresis and electroporation on the stratum corneum: review of the biophysical studies.* Adv. Drug Deliv. Rev., 35 (1999), pp. 89–105
2. T.J. Beverley, C.F. Barrie. *The transdermal revolution.* Drug Discov. Today, 9 (2004), pp. 697–703
3. C. Sinico, A.M. Fadda. *Vesicular carriers for dermal drug delivery.* Expert Opin. Drug Deliv., 6 (2009), pp. 813–825
4. M. Manconi, S. Mura, C. Sinico, A.M. Fadda, A.O. Vila, F. Molina. *Development and characterization of liposomes containing glycols as carriers for diclofenac.* Colloids Surf. A: Physicochem. Eng. Aspects, 342 (2009), pp. 53–58
5. M. Manconi, C. Sinico, C. Caddeo, A.O. Vila, D. Valenti, A.M. Fadda. *Penetration enhancer containing vesicles as carriers for dermal delivery of tretinoin.* Int. J. Pharm., 412 (2011), pp. 37–46
6. M. Manconi, C. Caddeo, C. Sinico, D. Valenti, M.C. Mostallino, G. Biggio, A.M. Fadda. *Ex vivo skin delivery of diclofenac by transcutol containing liposomes and suggested mechanism of vesicle–skin interaction.* Eur. J. Pharm. Biopharm., 78 (2011), pp. 27–35
7. S. Mura, M. Manconi, C. Sinico, D. Valenti, A.M. Fadda. *Penetration enhancer-containing vesicles (PEVs) as carriers for cutaneous delivery of minoxidil.* Int. J. Pharm., 380 (2009), pp. 72–79
8. S. Mura, M.Manconi, D.Valenti, C. Sinico, A.O. Vila, A.M. Fadda. *Transcutol containing vesicles for topical delivery of minoxidil.* J. Drug Target. , 19 (2011), pp. 189-196
9. M. Chessa, C. Caddeo, D. Valenti, M. Manconi, C. Sinico, A.M. Fadda. E*ffect of penetration enhancer containing vesicles on the percutaneous delivery of quercetin through new born pig skin.* Pharmaceutics (2011), pp. 497–509

10. C. Caddeo, M. Manconi, D. Valenti, A.M. Maccioni, A.M. Fadda, C. Sinico. *The role of Labrasol®in the enhancement of the cutaneous bioavailability of minoxidil in phospholipid Vesicles.* Res. J. Pharm. Technol. 5 (2012), pp 1563–1569
11. L. Tavano, R. Muzzalupo, S. Trombino, R. Cassano, A. Pingitore, N. Picci. *Effect of formulations variables on the in vitro percutaneous permeation of Sodium Diclofenac from new vesicular systems obtained from Pluronic triblock copolymers.* Colloids Surf. B: Biointerfaces, 79 (2010), pp. 227–234
12. S. Mura, M. Manconi, C. Sinico, D. Valenti, A.M. Fadda. P*enetration enhancer-containing vesicles (PEVs) as carriers for cutaneous delivery of minoxidil.* Int. J. Pharm., 380 (2009), pp. 72–79
13. C. Mura, A. Nácher, V. Merino, M. Merino-Sanjuan, C. Carda, A. Ruiz, M. Manconi, G. Loy, A.M. Fadda, O. Diez-Sales. *N-Succinyl-chitosan systems for 5-aminosalicylic acid colon delivery: in vivo study with TNBS-induced colitis model in rats.* Int. J. Pharm., 416 (2011), pp. 145–154
14. S. Scalia, M. Mezzena. *Incorporation of quercetin in lipid microparticles: effect of photo- and chemical-stability.* J. Pharm. Biomed. Anal., 49 (2009), pp. 90-94
15. L. Montenegro, C. Carbone, C. Maniscalco, D. Lambusta, G. Nicolisi, C.A. Ventura, G. Puglisi. *In vitro evaluation of quercetin-3-O-acyl esters as topical prodrugs.* Int. J. Pharm., 336 (2007), pp. 257-262
16. F.T. Vicentini, T.R. Simi, J.O. Del Ciampo, N.O. Wolga, D.L. Pitol, M.M. Iyomosa, M.V. Bentley, M.J. Fonseca. *Quercetin in w/o microemulsion: in vitro and in vivo skin damages evaluated in vivo.* Eur J. Pharm. Biopharm, 69(2008), pp. 948-957
17. H.H. Tonnesen, G. Smistad, T. Agren, J. Karlsen. *Studies on curcumin and curcuminoids: Effects of curcumin on liposomal lipid peroxidation.* Int. J. Pharm. 90 (1993), pp. 221–228
18. M. Subramanian, M.N. Sreejayan, T.P. Rao, B.B. Devasagayam. *Singh Dimi-*

nution of singlet oxygen-induced DNA damage by curcumin and related antioxidants. Mutat. Res. 311 (1994), pp. 249–255
19. R. Muzzalupo, L. Tavano, R. Cassano, S. Trombino, T. Ferrarelli, N. Picci. *A new approach for the evaluation of niosomes as effective transdermal drug delivery systems.* Eur. J. Pharm. Biopharm., 79 (2011), pp. 28–35
20. L. Tavano, R. Muzzalupo, R. Cassano, S. Trombino, T. Ferrarelli, N. Picci. *New sucrose cocoate based vesicles: preparation characterization and skin permeation studies.* Colloids Surf. B: Biointerfaces, 75 (2010), pp. 319–322
21. D. Cosco, C. Celia, F. Cilurzo, E. Trapasso, D. Paolino. *Colloidal carriers for the enhanced delivery through the skin.* Expert Opin. Drug Deliv., 5 (2008), pp. 737–755
22. M. Manconi, J. Aparicio, A.O. Vila, J. Pendás, J. Figueruelo, F. Molina. *Viscoelastic properties of concentrated dispersions in water of soy lecithin.* Colloids Surf. A: Physicochem. Eng. Aspects, 222 (2003), pp. 141–145
23. M. Manconi, J. Aparicio, D. Seyler, A.O. Vila, J. Figueruelo, F. Molina. *Effect of several electrolytes on the rheopectic behaviour of concentrated soy lecithin dispersions.* Colloids Surf. A: Physicochem. Eng. Aspects, 270–271 (2005), pp. 102–106
24. C. Caddeo, K. TeskaÄ, C. Sinico, J. Kristl. *Effect of resveratrol incorporated in liposomes on proliferation and UV-B protection of cells.* Int. J. Pharm., 363 (2008), pp. 183–191
25. G. Battaglia, A.J. Ryan. *The evolution of vesicles from bulk lamellar gels.* Nat. Mater., 4 (2005), pp. 869–876
26. G. Pabst, R. Koschuch, B. Pozo-Navas, M. Rappolt, K. Lohner, P. Laggner. *Structural analysis of weakly ordered membrane stacks.* J. Appl. Crystallogr., 36 (2003), pp. 1378–1388
27. R.V. McDaniel, T.J. McIntosh, S.A. Simon. *Nonelectrolyte substitution for*

water in phosphatidylcholine bilayers. Biochim. Biophys. Acta (BBA) – Biomembr., 731 (1983), pp. 97–108

28. R. Lee, S. Wang, M. Turk, P. Low. *The effects of pH and intraliposomal buffer strength on the rate of liposome content release and intracellular drug delivery.* Biosci. Rep., 18 (1998), pp. 69–78

29. M. Manconi, R. Isola, A.M. Falchi, C. Sinico, A.M. Fadda. *Intracellular distribution of fluorescent probes delivered by vesicles of different lipidic composition.* Colloids Surf. B: Biointerfaces, 57 (2007), pp. 143–151

30. M. Kranenburg, M. Vlaar, B. Smit. *Simulating induced interdigitation in mem-branes.* Biophys. J., 87 (2004), pp.1596–1605

31. R. Pignatello, V.D. Intravaia, G. Puglisi. *A calorimetric evaluation of the inter-action of amphiphilic prodrugs of idebenone with a biomembrane model.* J.Colloid Interf. Sci, 299 (2006), pp. 626–635

32. M.F.N. Rosser, H.M. Lu, P. Dea. *Effects of alcohols on lipid bilayers withand without cholesterol: the dipalmitoylphosphatidylcholine system.* Biophys.Chem, 81 (1999), pp. 33–44

33. T. Adachi, H. Takahashi, K. Ohki, I. Hatta. *Interdigitated structure of phospholipid–alcohol systems studied by X-ray diffraction.* Biophys. J. 68 (1995), pp 1850–1855

34. L. Löbbecke, G. Cevc. *Effects of short-chain alcohols on the phase behavior andinterdigitation of phosphatidylcholine bilayer membranes.* Biochim. Biophys.Acta (BBA) – Biomembranes, 1237 (1995), pp.59–69

35. C. Celia, E. Trapasso, D. Cosco, D. Paolino, M. Fresta. *Turbiscan Lab®expertanalysis of the stability of ethosomes®and ultradeformable liposomes containing a bilayer fluidizing agent.* Colloids Surf. B: Biointerf. 72 (2009), pp. 155–160

36. E. Touitou, N. Dayan, L. Bergelson, B. Godin, M. Eliaz. *Ethosomes novelvesicular carriers for enhanced delivery: characterization and skin penetrationproperties.* J. Control. Release, 65 (2000), pp. 403–418
37. H. Komatsu, S. Okada. *Increased permeability of phase-separated lipo-somal membranes with mixtures of ethanol-induced interdigitated andnon-interdigitated structures.* Biochim. Biophys. Acta (BBA) Biomem, 1237 (1995), pp. 169–175
38. R. Elmoslemany, O. Abdallah, L. El-Khordagui, N. Khalafallah. *Propylene glycol liposomes as a topical delivery system for miconazole nitrate: comparison with conventional liposomes.* AAPS PharmSciTech 13 (2012), pp. 723–731
39. M.M.A. Elsayed, O.Y. Abdallah, V.F. Naggar, N.M. Khalafallah. *PG-liposomes:novel lipid vesicles for skin delivery of drugs.* J. Pharm. Pharmacol. 59 (2007), pp. 1447–1450
40. M. Manconi, C. Caddeo, C. Sinico, D. Valenti, M.C. Mostallino, S. Lampis, M. Monduzzi, A.M. Fadda. *Penetration enhancer-containing vesicles: compositiondependence of structural features and skin penetration ability.* Eur. J. Pharm.Biopharm, 82 (2012), pp. 352–359
41. E. Escribano, A.C. Calpena, J. Queralt, R. Obach, J. Doménech. *Assessment ofdiclofenac permeation with different formulations: anti-inflammatory study of a selected formula.* Eur. J. Pharm. Sci. 19 (2003), pp. 203–210
42. O. López, M. Cócera, R. Pons, H Amenitsch, J. Caelles, J.L. Parra, L. Coderch, A. de la Maza. *Use of synchrotron radiation SAXS to study the first steps of theinteraction between sodium dodecyl sulfate and charged liposomes.* Spectrosc.Int. J. 16 (2002), pp. 343–350
43. S. Schreier, S.V.P. Malheiros, E. de Paula. *Surface active drugs: self-associationand interaction with membranes and surfactants. Physicochemical and biolog-ical aspects.* Biochim. Biophys. Acta (BBA) – Biomembranes, 1508 (2000), pp. 210–234

44. S. Madrigal-Carballo, D. Seyler, M. Manconi, S. Mura, A.O. Vila, F. Molina. *An approach to rheological and electrokinetic behaviour of lipidic vesicles cov-ered with chitosan biopolymer.* Colloids Surf. A Physicochem. Eng. Aspects, 323 (2008), pp. 149–154
45. J.C.M. Stewart. *Colorimetric determination of phospholipids with ammoniu-mferrothiocyanate.* Anal. Biochem., 104 (1980), pp. 10–14
46. G. Pabst, M. Rappolt, H. Amenitsch, P. Laggner. *Structural information frommultilamellar liposomes at full hydration: full q-range fitting with high qualityX-ray data.* Phys. Rev., E 62 (2000), pp. 4000–4009
47. L.B. Lopes, M.V. Scarpa, G.V.J. Silva, D.C. Rodrigues, C.V. Santilli, A.G. Oliveira. *Studies on the encapsulation of diclofenac in small unilamellar liposomes of soyaphosphatidylcholine.* Colloids Surf. B: Biointerf, 39 (2004), pp. 151–158
48. L. Tavano, R. Muzzalupo, S. Trombino, R. Cassano, A. Pingitore, N. Picci. *Effect of formulations variables on the in vitro percutaneous permeation ofsodium diclofenac from new vesicular systems obtained from pluronic triblockcopolymers.* Colloids Surf. B Biointerf., 79 (2010), pp. 227–234
49. W. Schtze, C.C. Ller-Goymann. *Phase Transformation of a Liposoma Disper-sion into a Micellar Solution Induced by Drug-Loading.* Springer, New York, NY,ETATS-UNIS.Simon,
S.A., McIntosh, T.J., 1984. *Interdigitated hydrocarbon chain packing causesthe bi-phasic transition behavior in lipid/alcohol suspensions.* Biochim. Biophys. Acta (BBA) – Biomembranes, 773 (1998), pp. 169–172
50. Z. Abramovic, U. Sustarsic, K. Teskac, M. Sentjurc, J. Kristl. *Influence of nano-sized delivery systems with benzyl nicotinate and penetration enhancers on skinoxygenation.* Int. J. Pharm, 359 (2008), pp. 220–227
51. M. Manconi, F. Marongiu, G. Ennas, A. Scano, C. Sinico, D. Valenti, A.M.

Fadda. *Liposomes for (trans)dermal delivery of tretinoin: influence of drug con-centration and vesicle composition.* J. Drug Deliv. Sci. Technol, 18 (2008), pp. 309–313
52. E. Feitosa, P.C.A. Barreleiro, G. Olofsson. *Phase transition in dioctade-cyl-dimethylammonium bromide and chloride vesicles prepared by differentmethods.* Chem. Phys. Lipids 105 (2000), pp. 201–213
53. U. Vierl, L. Löbbecke, N. Nagel, G. Cevc. *Solute effects on the col-loidal and phase behavior of lipid bilayer membranes: ethanol–dipalmitoyl-phosphatidyl-choline mixtures.* Biophys. J., 67 (1994), pp. 1067–1079
54. J.K. Prasain, S. Barnes. *Metabolism and Bioavailability of Flavonoids in Chemoprevention: Current Analytical Strategies and Future Prospectus.* Molecular Pharmaceutics, 4 (2007), pp. 846-864
55. T.-T. Phan, P. See, S.-T. Lee, S.-Y. Chan. *Protective Effects of Curcumin against Oxidative Damage on Skin Cells In Vitro: Its Implication for Wound Healing.* The Journal of Trauma and Acute Care Surgery, 51 (2001), pp. 927-931
56. M. Panchatcharam, S. Miriyala, V. Gayathri L. Suguna. *Curcumin improves wound healing by modulating collagen and decreasing reactive oxygen species.* Mol Cell Biochem, 290 (2006), pp. 87-96
57. I. Appleton Wound healing: future directions. IDrugs : the investigational drugs journal, 6 (2003), pp. 1067-1072
58. J.A. Nichols, S.K. Kativar. *Skin photoprotection by natural polyphenols: anti-inflammatory, antioxidant and DNA repair mechanisms.* Springer, Heidelberg, Germany, 2010
59. M.M. Yallapu, M. Jaggi, S.C. Chauhan. *Curcumin nanoformulations: a future nanomedicine for cancer.* Drug Discovery Today, 17 (2012), pp. 71-80
60. C. Caddeo, M. Manconi, A.M. Fadda, F. Lai, S. Lampis, O. Diez-Sales, C. Sinico. *Nanocarriers for antioxidant resveratrol: formulation approach, vesicle self-as-*

sembly and stability evaluation. Colloids and Surfaces B: Biointerfaces, 111 (2013), pp. 327-332

61. D. Pando, C. Caddeo, M. Manconi, A.M. Fadda , C. Pazos. *Nanodesign of olein vesicles for the topical delivery of the antioxidant resveratrol.* Journal of Pharmacy and Pharmacology, (2013) 10.1111/jphp.12093

62. C. Mohanty, M. Das, S.K. Sahoo. *Sustained Wound Healing Activity of Curcumin Loaded Oleic Acid Based Polymeric Bandage in a Rat Model.* Molecular Pharmaceutics, 9 (2012), pp. 2801-2811

63. K. Gomathi, D. Gopinath, M. Rafiuddin Ahmed, R. Jayakumar. *Quercetin incorporated collagen matrices for dermal wound healing processes in rat.* Biomaterials, 24 (2003), pp. 2767-2772

64. D. Gopinath, M.R. Ahmed, K. Gomathi, K. Chitra, P.K. Sehgal, R. Jayakumar. *Dermal wound healing processes with curcumin incorporated collagen films, Biomaterials.* 25 (2004), pp. 1911-1917

65. I.P. Süntar, E.K. Akkol, F.N. Yalçın, U. Koca, H. Keleş, E. Yesilada. *Wound healing potential of Sambucus ebulus L. leaves and isolation of an active component, quercetin 3-O-glucoside.* Journal of Ethnopharmacology, 129 (2010), pp. 106-114

66. A. Martin. *The Use of Antioxidants in Healing.* Dermatologic Surgery, 22 (1996), pp. 156-160

67. C. Caddeo, O.D. Sales, D. Valenti, A.R. Saurí, A.M. Fadda, M. Manconi. *Inhibition of skin inflammation in mice by diclofenac in vesicular carriers: Liposomes, ethosomes and PEVs.* International Journal of Pharmaceutics, 443 (2013), pp. 128-136

68. H. Sato, I. Sugimoto, T. Matsunaga, M. Tsuchimoto, T. Ohta, H. Uno, M. Kiyoki. *Tacalcitol (1,24(OH)2D3, TV-02) inhibits phorbol ester-induced epidermal proliferation and cutaneous inflammation, and induces epidermal differentiation in mice.* Arch Dermatol Res, 288 (1996), pp. 656-663

69. R.H. Liu. *Health benefits of fruit and vegetables are from additive and synergistic combinations of phytochemicals.* The American journal of clinical nutrition, 78 (2003), pp. 517S-520S
70. J.M. Davis, E.A. Murphy, M.D. Carmichael. *Effects of the Dietary Flavonoid Quercetin Upon Performance and Health.* Current Sports Medicine Reports, 8 (2009), pp. 206-213
71. Martin. *The use of antioxidants in healing.* Wiley, Malden, MA, ETATS-UNIS, 1996.
72. G.S. Sidhu, A.K. Singh, D. Thaloor, K.K. Banaudha, G.K. Patnaik, R.C. Srimal, R.K. Maheshwari. *Enhancement of wound healing by curcumin in animals.* Wound Repair and Regeneration, 6 (1998), pp. 167-177
73. C.H. Purdon, C.G. Azzi, J. Zhang, E.W. Smith, H.I. Maibach. *Penetration Enhancement of Transdermal Delivery-Current Permutations and Limitations.* Critical Reviews™ in Therapeutic Drug Carrier Systems, 21 (2004), pp. 97-132
74. M. Manconi, S. Mura, C. Sinico, A.M. Fadda, A.O. Vila, F. Molina. *Development and characterization of liposomes containing glycols as carriers for diclofenac.* Colloids and Surfaces A: Physicochemical and Engineering Aspects, 342 (2009), pp. 53-58
75. S.H. Moghadam, E. Saliaj, S.D. Wettig, C. Dong, M.V. Ivanova, J.T. Huzil, M. Foldvari. *Effect of Chemical Permeation Enhancers on Stratum Corneum Barrier Lipid Organizational Structure and Interferon Alpha Permeability.* Molecular Pharmaceutics, 10 (2013), pp. 2248-2260
76. W.-C. Hung, F.-Y. Chen, C.-C. Lee, Y. Sun, M.-T. Lee, H.W. Huang. *Membrane-Thinning Effect of Curcumin.* Biophysical Journal, 94 (2008), pp. 4331-4338
77. A.D. Petelska, Z.A. Figaszewski. *Interfacial tension of phosphatidylcholine–phosphatidylserine system in bilayer lipid membrane.* Biophysical Chemistry, 120

(2006), pp. 199-206
78. H.F. Frasch, A.M. Barbero. *A paired comparison between human skin and hairless guinea pig skin in vitro permeability and lag time measurements for 6 industrial chemicals.* Cutaneous and Ocular Toxicology, 28 (2009), pp. 107-113
79. F. Cilurzo, P. Minghetti, C. Sinico. *Newborn pig skin as model membrane in in vitro drug permeation studies: A technical note.* AAPS PharmSciTech, 8 (2007), pp. 97-100
80. Y. Liu, J.Y. Chen, H.T. Shang, C.E. Liu, Y. Wang, R. Niu, J. Wu, H. Wei. *Light microscopic, electron microscopic, and immunohistochemical comparison of Bama minipig (Sus scrofa domestica) and human skin.* Comparative medicine, 60 (2010), pp 142-148
81. S.M. San Miguel, L.A. Opperman, E.P. Allen, J. Zielinski, K.K.H. Svoboda. *Bioactive polyphenol antioxidants protect oral fibroblasts from ROS-inducing agents.* Archives of Oral Biology, 57 (2012), pp. 1657-1667
82. S.J. Kim, M.H. Lim, I.K. Chun, Y.H. Won. *Effects of Flavonoids of Ginkgo biloba on Proliferation of Human Skin Fibroblast.* Skin Pharmacology and Physiology, 10 (1997), pp. 200-205
83. R.K. Maheshwari, A.K. Singh, J. Gaddipati, R.C. Srimal. *Multiple biological activities of curcumin: A short review.* Life Sciences, 78 (2006), pp. 2081-2087
84. A.S. Michaels., S.K. Chandrasekaran, J.E. Shaw. *Drug permeation through human skin: theory and in vitro experimental measurement.* AIChE J. 21 (1975), pp. 985–996.